**Title**

Hybrid System Combining Two-Dimensional Materials and Ferroelectrics and Its Application in Photodetection

**Journal**

ACS Nano, 15(7)

**ISSN**

1936-0851

**Authors**

Sun, Yanxiao
Niu, Gang
Ren, Wei
et al.

**Publication Date**

2021-07-27

**DOI**

10.1021/acsnano.1c01735

DOI: 10.1002/ ((please add manuscript number))

**Article type:** **Review**

# Photodetectors Based on Hybrid Systems Combining Two-dimensional materials and Ferroelectrics

*Yanxiao Sun*[1], *Gang Niu*[1]*, *Wei Ren*[1], *Xiangjian Meng*[2], *Jinyan Zhao*[1], *Wenbo Luo*[3], *Zuo-Guang Ye*[4], *Ya-Hong Xie*[5]

1. Electronic Materials Research Laboratory, Key Laboratory of the Ministry of Education & International Center for Dielectric Research, School of Electronic Science and Engineering, Xi'an Jiaotong University, No. 28, Xianning West Road, Xi'an, Shaanxi, 710049, P.R. China
E-mail: gangniu@xjtu.edu.cn
2. National Laboratory for Infrared Physics, Shanghai Institute of Technical Physics, Chinese Academy of Sciences, Shanghai, China
3. State Key Laboratory of Electronic Thin Films and Integrated Devices, University of Electronic Science and Technology of China, Chengdu, 611731 China
4. Department of Chemistry and 4D LABS, Simon Fraser University, Burnaby, British Columbia, V5A 1S6, Canada
5. Department of Materials Science and Engineering, University of California, Los Angeles, Los Angeles, California, United States

Keywords: two-dimensional materials; ferroelectrics; photodetectors; hybrid systems

Two-dimensional materials have been extensively studied in last decades due to their remarkable physical, electrical and optoelectronic properties. Meanwhile, combination of two-dimensional materials with traditional functional materials have provided new approach in a variety of research and application areas. In this review, we have focused on the two-dimensional and ferroelectric hybrid system being applied in photodetection. Fundamentals of the materials and interaction in the hybrid system was introduced. Modulation of the optoelectronic properties induced by ferroelectricity was discussed in the hybrid system. After introducing the basics of photodetection, the devices were categorized and reviewed based on their structures. Modulation and enhancement of the photodetectors were observed with ferroelectric polarization. Finally, the challenges and perspectives of the photodetectors based on two-dimensional materials and ferroelectrics have been proposed.

## 1. Introduction

Last decades have witnessed rapid development of photonic and optoelectronic devices which demonstrate a wide spectrum of applications including photo-emission (eg. photodiodes[1, 2, 3, 4], LEDs[5, 6] and lasers[7, 8]), photodetection[9, 10, 11, 12, 13], data storage[14, 15] and energy storage[16, 17]. Nowadays, the information society featuring “Internet of Things” and “big data” demands further evolution of electronics and optoelectronics, particularly for telecommunication and communication. Photodetectors, serving as the receiving end, are one of the most important components in such optic communication network. [18] Photodetectors are among the most ubiquitous devices with superiorities of the sufficiently fast response, the high detectivity, the remarkable data storage capability etc. Photodetectors detect light in a certain range of frequency band and the device performance can be evaluated by a series of figures of merit, which are dominated by the device structure and more importantly by detecting materials. Among the massive materials and devices applied in the photodetection, semiconductor-based photodetectors have attracted intense interest from both academic and industrial fields, thanks to their smaller size, wide band detection and Si-technology compatibility. These photodetectors could be tailored by simply altering the composition of the various layers forming the structure. Both individual devices and the component in the communication system requires compact structure, ultra-thin devices and further optimization of the opto-electronic properties, which has triggered the flourishing of novel materials with outstanding structure and properties.

Conventional materials applied in electronic and optoelectronic semiconductor devices are crystalline silicon (Si) and germanium (Ge). Compounds of III-V semiconductors such as Gallium (Ga), Indium (In), Arsenic (As), Phosphorus (P) and antimony (Sb) are also applied in the materials as well as the alloys due to their direct bandgap property and have been intensively studied for years.[19, 20, 21] More recently, with the advent of two-dimensional (2D) materials,[22, 23] various new photodetection phenomenon have been reported due to their mechanical, thermal, electrical, optical and optoelectronic properties distinguished from that of the three-dimensional counterparts, [24, 25, 26] which has made a tremendous progress of photodetectors. Materials with Van der Waals bonds interlayers usually form thick bulk or crystals which makes them difficult utilized in nanodevices. Such obstacle was overcome by the Novoselov and Geim in 2004, who successfully exfoliated the graphene nano flake and applied it in a field-effect transistor (FET) for ultrafast photodetection.[27, 28] Since then, 2D materials have rapidly been established as building blocks for photodetectors due to their remarkable optical and optoelectronic properties.[29, 30, 31] Fabrication procedure of 2D materials photodetectors is quite simple, which as well provides a facile platform for micro- and nano- devices fabrication.[32, 33] In general, 2D materials are potential in building highly integrated and efficient photodetectors, and promising candidate for the future integrated optoelectronic devices as well.

The library of 2D materials has experienced a gradual expansion from graphene to its derivatives (eg. graphene, carbon nano tubes (CNTs), hexagonal boron nitride (h-BN), and to

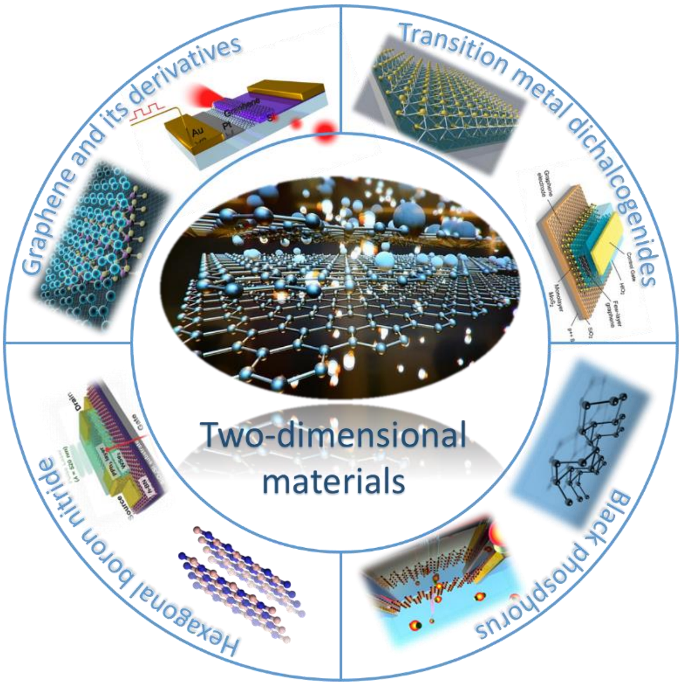

**Figure 1.** Categories of 2D materials and their applications in electronics and optoelectronics.[34, 35, 36] Copyright Year, Publisher.

layered group-IV and group-III metal chalcogenides, as well as to layered transition metal dichalcogenides (TMDs) with their alloys and heterostructures and other novel functional materials etc., as summarized in Figure 1.[34, 35, 36] With the growth of 2D materials family, they have covered from metal, semiconductor to insulators now. 2D materials have ultra-thin physical structure ranging from ~0.4 nm (one monolayer) to bulk materials with tens of nanometers. Some 2D materials, like graphene and TMDs, show a typical bandgap transition with the thickness variation, which provide opportunities for bandgap modulation. [37] Meanwhile, Electrical and optoelectronic properties of the 2D materials are closely related to the band structure, which corresponding to the thickness variation and bandgap modulation in 2D materials.[38] Furthermore, The atomic-scale thickness of 2D materials leads to the high transparency and flexibility, which is of particular interest in novel wearable, flexible and portable devices.

Meanwhile, another category of materials being employed in electronic and optoelectronic devices are functional materials, also known as “smart materials”, with typical properties responding to the external stimuli. [39] Functional materials are capable of coupling the input (eg. electric field, magnetic field, stress, light field and heat) and output (eg. charge/current, magnetization, strain, light and temperature), as shown in Figure 2.[40] The “smart materials” nowadays are widely applied in actuators, sensors and detectors. Among smart materials, ferroelectrics is unique due to its spontaneous reversal of polarization with switching of external electric field. Main application areas of ferroelectrics include energy harvesting, memory devices and data storage devices.[41, 42, 43, 44]. More and more electronic devices and photodetectors with profound performances are achieved with ferroelectric materials employed. [45]

Photodetection could be realized with ferroelectrics as active layers, where polarization of the materials could be altered by the incident light, resulted in linear, nonlinear optical or electrical output. Furthermore, polarization of the ferroelectrics enables wavelengths modulation by altering of the applied polarization direction. Both inorganic ferroelectric materials like $Pb(Zr,Ti)O_3$ (PZT),[46, 47, 48, 49] $BaTiO_3$ (BTO),[50, 51] $LiNbO_3$ (LN),[52, 53] $BiFeO_3$ (BFO)[54, 55, 56] and organic compounds PVDF as well as the derivatives[57, 58]have been studied and applied in photodetectors. Nevertheless, ferroelectrics can only response to limited frequency band width of light, for other incident light to which ferroelectrics are unable to response, other group of the materials could be introduced. 2D materials, which are known for their wide band response could combine with ferroelectric layers. Such hybrid photodetection systems might probably lead to new phenomena and therefore become a topic attracting increasing studies. As for the photodetectors, the hybrid structure could modulate the carriers and performance of the devices could be optimized.

In addition to the materials chosen in photodetection, structure of the devices is also of vital importance. Grouped by structures, photodetectors include devices like phototubes,

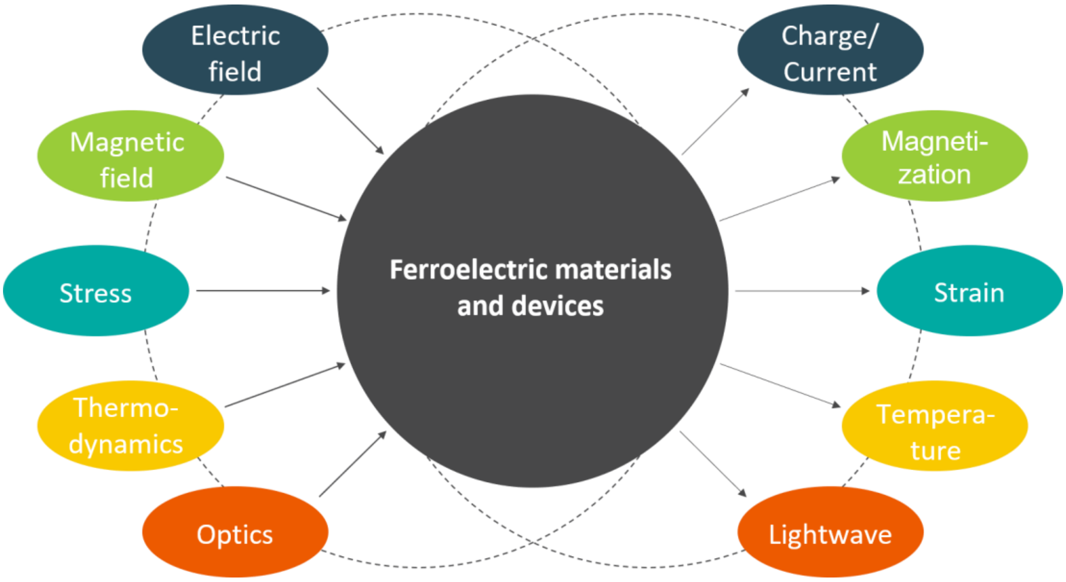

**Figure 2.** Coupling of the fields in ferroelectric materials and devices

photomultipliers and semiconductor photodetectors. Phototubes and photomultipliers are mostly applied as dependent devices. As for the semiconductor photodetectors, one of the most prominent advantages is its capability of been compacted into integrated circuits. Furthermore, photodetection arrays could thus been achieved. Basic structures of the semiconductor photodetectors could be categorized into PN diodes, Schottky diodes as well as field effect transistors *etc*..

In this work, we review the structures and devices based on ferroelectrics and 2D materials hybrid system for photodetection. Fundamentals of the 2D materials and ferroelectrics including structure, electrical, optoelectronic and interaction of the hybrid system are presented. After that, various structures and corresponding nano devices for photodetection are discussed in detail, including PN junctions, field effect transistors and other types of devices. Performances of the hybrid devices was summarized and discussed. This review outlines the important aspects of the ferroelectrics-2D materials hybrid photodetectors and is certainly of great interest for design novel photodetectors.

## 2. Fundamentals of 2D materials and ferroelectrics

### 2.1. Fundamentals of 2D materials

Exfoliation of the monolayer graphene has opened the door to research 2D materials. Monolayer graphene was applied in the FET and the outstanding electrical and structure property were observed. With deep exploration of graphene and its relative derives, as well as other 2D materials with similar structure for instance the hexagonal-boron nitride (h-BN), TMDs and black phosphorus (BP). These novel 2D materials share excellent optical and optoelectronic properties, which attracting more research for optoelectronic devices.

### 2.1.1. Graphene

It was convinced that nano-materials were hardly remain stable due to thermal fluctuation, which consequently lead to decomposition of the materials. In this case, the thermally stable and chemically inert graphene has brought big surprise to scientist, leading to booming development of 2D materials research area in the past decades.[33, 59, 60] Researchers tried to add the "fresh blood" into the "old fashioned" methods, devices and systems to create novel structures and to improve the performance.

Graphene has in-plane chemistry bond connecting the atoms and can stack with Van der Waals forces between layers. The structure of graphene is hexagonal arrangement of $sp^2$-bonded carbon atoms with zero bandgap and Dirac point. In graphene, single layer of carbon atoms with $sp^2$-hybridization arranged in a honeycomb lattice, which is just one atom thick at vertical dimension (about 0.14 nm). Each carbon atom in-plane bonds to other three nearest atoms with a distance of 1.42 Å, shown in Figure 3.[61] The lattice of graphene can be considered as two interpenetrating triangular sub-lattice A and B, see in Figure 4(a). Band structure in graphene materials could be modeled by the tight-binding approximation as well as calculated based on the first principle.[62, 63, 64], as shown in Figure 4(b) and (c).

The $p_z$ orbitals remained, which do not involve in the covalent bonding, is responsible for the electric conductivity. Graphene is a promising candidate for electronic devices with outstanding electrical properties. Conductivity and mobility of the graphene nanosheets

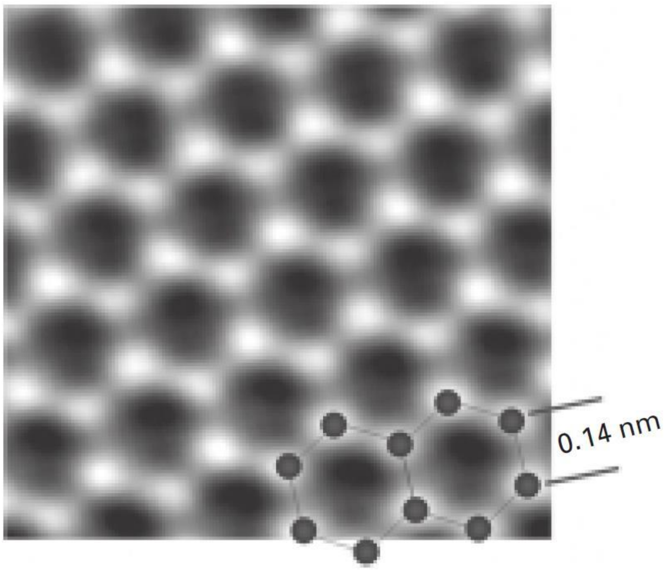

**Figure 3.** Atomic structure of graphene nanosheets demonstrated the bond between the atoms and the honeycomb structure of the graphene layer (courtesy of Berkeley's TEAM05, 2009).

mostly depend on the defect scattering process, which is almost independent from temperature. [65] The minimum conductivity of graphene theoretically exhibits at the Dirac point as $4e^2/\pi h$. The electron mobility ranges from ~$0.67\times10^4$ $cm^2V^{-1}s^{-1}$ up to $10^6$ $cm^2V^{-1}s^{-1}$ in the form of suspended nanosheets or supported by $SiO_2$/Si substrates. [30, 66, 67] Meanwhile, high current carrying capacity of ~$5.8\times10^6$ $A\cdot cm^{-2}$ and ~$1.8\times10^9$ $A\cdot cm^{-2}$ in graphene/Cu nano-composite wires and on synthetic diamond substrate, respectively.[68, 69, 70] Such high current carrying capacity is particularly feasible for the energy storage system and device minimization. Additionally, high thermal conductivity ranging from ~4840 W/m·K to 5300 W/m·K has been observed in layered graphene nanosheets, indicating their outstanding heat dissipation capability, which can be beneficial for batteries and thermal conductive devices. [71]Relative low contact resistance 100 Ω·µm between graphene and metal electrodes allows the application of electronic devices with low Schottky barrier height.[72] Graphene is different from conventional metals not only due to its 2D structure and transparency in a wide band incident light but also because of its ambipolar field effect transport property. Graphene is consequently known as the "semimetal".[73, 74, 75, 76, 77, 78]

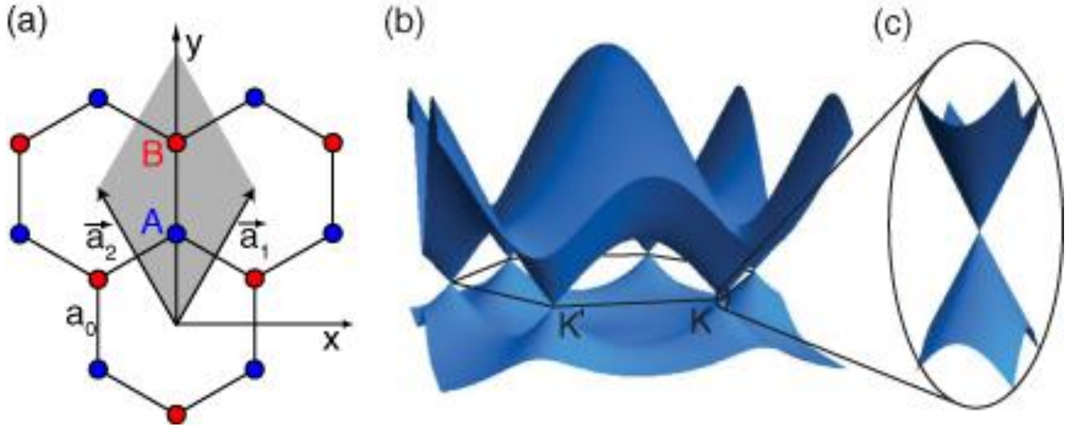

**Figure 4.** (a) lattice, (b) band structure and (c) zero-bandgap achieved by tight-binding approximation

As the zero-band gap structure, graphene should theoretically be capable of responding to all the photons, which consequently leads to the advantage of wide band detection from ultraviolet to infra-red and all the way to Terahertz region.[31, 79, 80] In addition to the wide band response properties, pristine monolayer graphene is of high transparency, with absorption of 2.3% in a wide band. [81] Such high transmittance brings the opportunity for graphene being applied as transparent electrodes, especially for those allow large absorption area. Moreover, broad band absorption of graphene could be modulated by shifting the electronic Fermi level, which could consequently dominate the photon transition in graphene nanosheets.[82, 83] With interaction of incident light, energy could be converted among carriers, photons and phonons in graphene by transition of the charge carriers (electrons and holes). Macroscopic phenomena such as photon absorption,[84, 85] nonlinear optical properties[86, 87, 88], plasmons,[89, 90] and photo-current have been observed.

### 2.1.2. Transition Metal Dichalcogenides

Another group of 2D materials with intrinsic bandgap and similar electrical properties, as well as optoelectrical properties with graphene are TMDs. TMDs with chemical formula $MX_2$, is a group of materials composed of transition metal (eg. Mo, W, etc.) and chalcogen (eg. S, Se, Te, etc.), as shown in Figure 5. TMDs share similar structures that can be categorized into

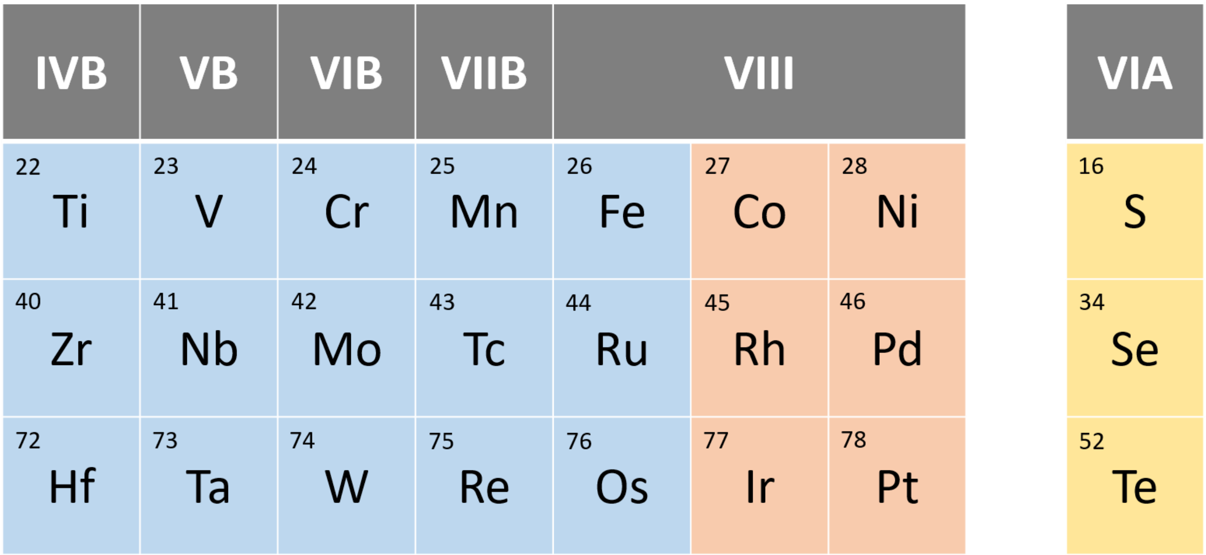

| IVB | VB | VIB | VIIB | VIII | | | VIA |
|---|---|---|---|---|---|---|---|
| 22<br>Ti | 23<br>V | 24<br>Cr | 25<br>Mn | 26<br>Fe | 27<br>Co | 28<br>Ni | 16<br>S |
| 40<br>Zr | 41<br>Nb | 42<br>Mo | 43<br>Tc | 44<br>Ru | 45<br>Rh | 46<br>Pd | 34<br>Se |
| 72<br>Hf | 73<br>Ta | 74<br>W | 75<br>Re | 76<br>Os | 77<br>Ir | 78<br>Pt | 52<br>Te |

**Figure 5.** Elements for TMDs. The ones marked in orange means only some of the compounds can form int layered structures

several polytypes varying in stacking orders and metal atom coordination, as shown in Figure 6.[91] The 2H, 3R and 1T phases are the most stable and common structure of TMDs, among which 1H is the most stable and the most studied structure. 3R and 1T phase are metastable and can be converted into 2H by annealing, heating or laser excitation. [92, 93] Properties of different compounds varies at conductivity. For example, compounds with M=Mo and W, X=Se and S are semiconducting,[94, 95, 96] while with M=Nb and Ta are metallic.[97] TMDs experience the transition of indirect bandgap to direct optical bandgap with the number of layers decreased to bilayer or monolayer, as shown in Figure 7.[98] The bandgap ranges from 1.0 eV to 2.1 eV, see in Table 1. Some of the TMDs, like TiS$_2$ and WT$_2$, show zero bandgap structure, being similar to graphene. Bandgap modulation is desired for applications of TMDs in nano-devices under certain circumstances due to the requirement of tunable electronic properties. Therefore, bandgap modulation by strain engineering, electric field control, alloying and hybrid system fabrication has been studied.

MoS$_2$ is considered as a typical representative TMD and has been recently intensively studied. MoS$_2$ has transition bandgap of 1.2 eV~1.9 eV with the thickness decreased from bulk or few-layer to monolayer. The optical properties of MoS$_2$ depends on its bandgap structures. With

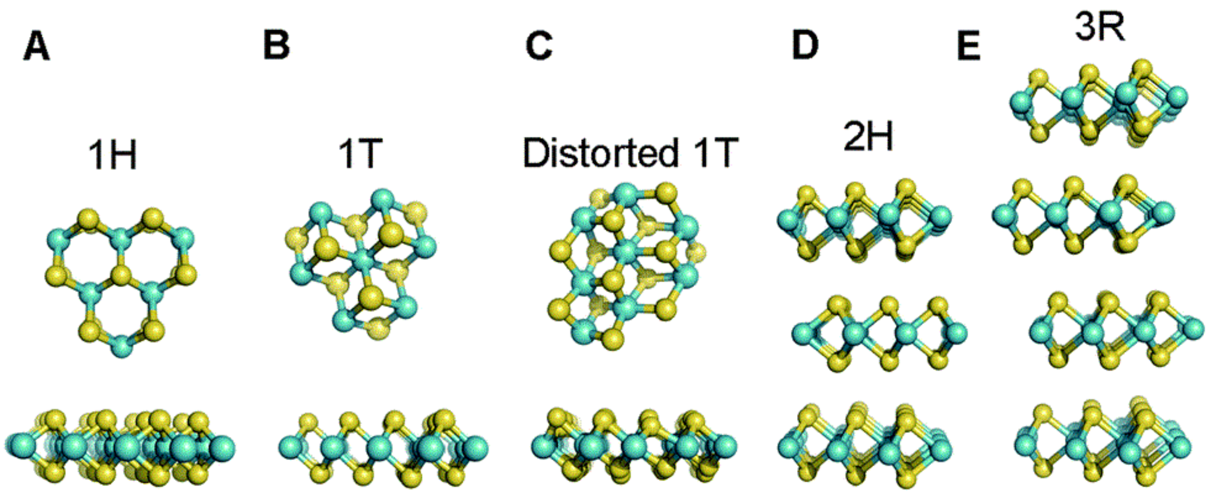

**Figure 6.** structures of the TMDs.

bandgap ranges from 1.2 eV to 1.9 eV, corresponding to wavelengths ranging from 652.6 nm to 1033.3 nm. Linear absorption in the valence band occurs with incident light whose photon energy is higher than 1.2 eV. Photocurrent is generated from the electrons in the conductive band, as shown in Figure 8. Such optoelectronic property and the electrical conductance, as well as carrier mobility of $MoS_2$ nanosheets show great potential in photodetection with wide band response and high sensitivity.

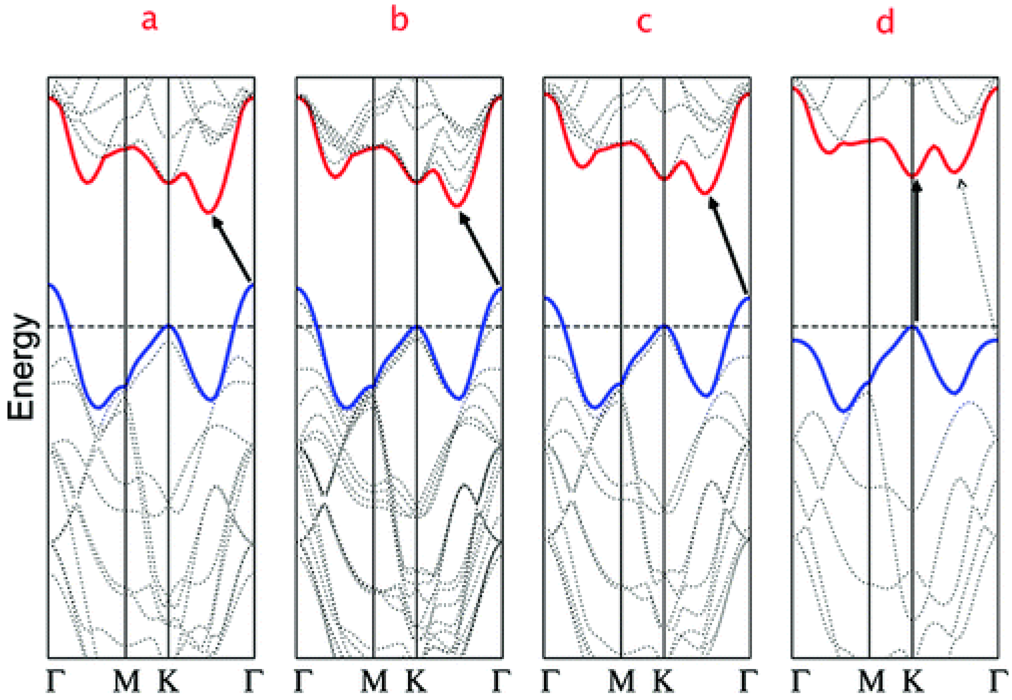

**Figure 7.** Electrical properties of the layered $MoS_2$

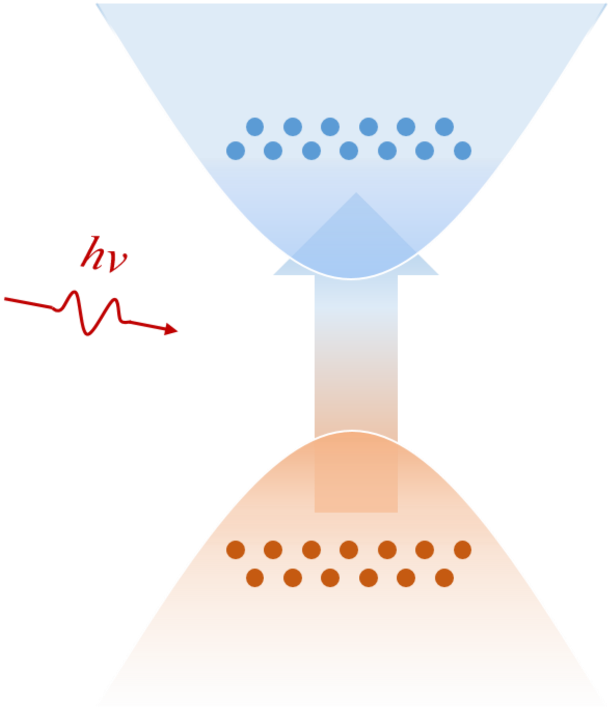

**Figure 8.** Non-equilibrim carrier generated by incident light

2.1.3. Other novel 2D materials

Recently 2D materials composed of group-IV (Si, Ge and Sn) elements have also emerged. Silicene and germanene has similar structure as graphene with honeycomb lattice arranged in-plane and Van der Waals bond between adjacent layers. They have application potential in the integrated circuits due to their Si-technology compatibility. Another group IV atomic material that has been intensively studied is stanine whose structure also resembles graphene with two common allotropes: α-tin with face-centered cubic lattice like diamond and β-tin with face-centered tetragonal lattice.

Another category of novel 2D materials, the black phosphorus (BP), was first synthesized a century ago and recently attracts lots of interest due to its direct bandgap in bulk and monolayer ranges from 0.33 eV to >1 eV. BP could thus be applied in the mid-infrared photodetectors. Scotch tape method could achieve exfoliated monolayer BP and thickness of monolayer BP could be 0.7-0.85 nm. Structure of the BP is shown in Figure 9. As for the electric properties of BP, the electron and hole mobilityS were measured to be >1000 cm$^2$V$^{-1}$s$^{-1}$ at room temperature with high on/off ratio in the application and on/off ratio, together with its band structure, making it suitable for photodetection.[100, 101]

## 2.2. Fundamentals of ferroelectrics

Ferroelectrics are a group of materials with asymmetry lattice structure, resulting in dipoles in the lattice and capable of being modulated by the external stimuli. One of the most typical characteristics of ferroelectrics is the spontaneous polarization, i.e. the positive and negative charge centers in the original cell of the lattice do not coincide without external electric field

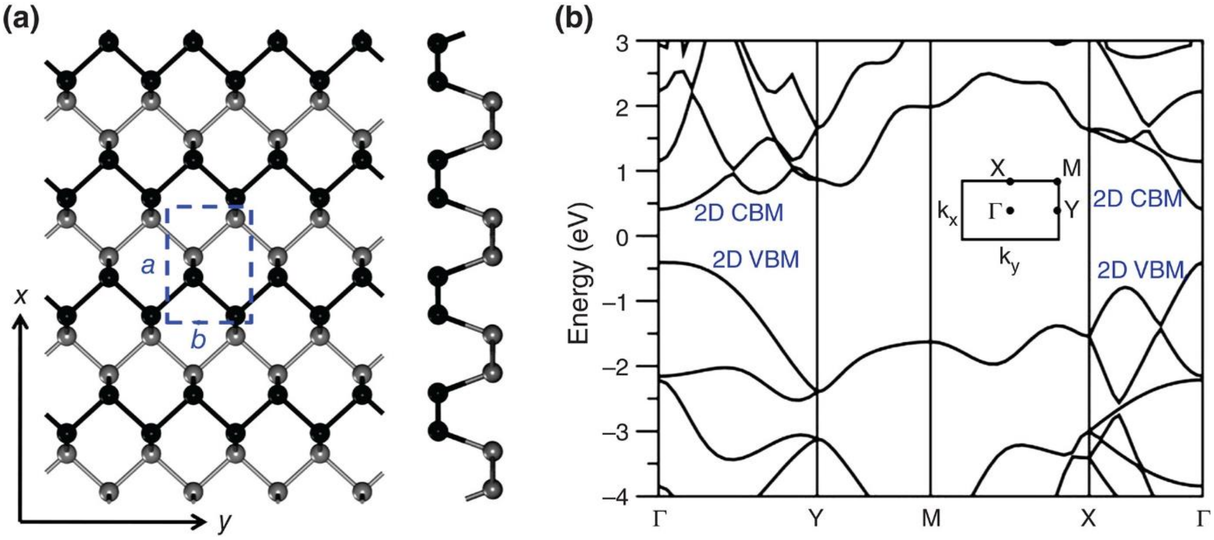

**Figure 9.** (a) Lattice structure and (b) electrical band structure of phosphorene.

**Table 1.** Bandgap of typical $MX_2$ (M=Mo, W; X=S, Se, Te)

| TMDs | Number of layers | Band gap [eV] | Reference |
|---|---|---|---|
| $MoS_2$ | monolayer | 1.9-1.95 | [150, 151] |
| $MoS_2$ | bulk | 1.20-1.29 | [98, 152, 153] |
| $MoSe_2$ | monolayer | 1.44-1.55 | [154, 155] |
| $MoSe_2$ | bulk | 1.1 | [154] |
| $WS_2$ | monolayer | 1.80-2.05 | [155, 156, 157] |
| $WS_2$ | bulk | 1.30-1.35 | [153, 158] |
| $WSe_2$ | monolayer | 1.65-1.70 | [159, 160] |
| $WSe_2$ | bulk | 1.2 | [161] |
| $MoTe_2$ | monolayer | 0.90-1.10 | [162, 163, 164, 165] |
| $MoTe_2$ | bulk | 0.88 | [164, 165] |
| $WTe_2$ | monolayer | 0.18 | [166, 167] |
| $WTe_2$ | bulk | 0.7-0.81 | [166, 168] |

within a certain temperature range. Other properties including the dielectricity, piezoelectricity, pyroelectricity and related effects (for instance electro-optical effect, acoustic-optical effect, photorefractive effect as well as nonlinear optical properties) make them particularly suitable for varieties of applications. These phenomena related to the lattice structure of ferroelectrics could be further investigated by “ferroelectric domain” structure in the materials. Domains are defined as small region of lattice with the same polarization direction, which is correlated to the lattice asymmetry, piezoelectricity and ferroelectricity of the materials. According to the lattice structure, ferroelectrics are categorized into perovskite, pyrochlores, the tungsten-bronze group and the bismuth layer structure group. In combination with 2D materials, the ferroelectrics could be applied as the functional layer due to the alter of polarization with external electric field switching. Typical ferroelectrics including inorganic perovskites with $ABO_3$ structure, like $Pb(Zr,Ti)O_3$ (PZT), $PbTiO_3$ (PT), $Pb(Mg,Nb)O_3$-$PbTiO_3$ (PMN-PT), $BaTiO_3$ (BTO), $(Bi,Na)TiO_3$-$BaTiO_3$ (BNT-BT), (K, Na)$NbO_3$ (KNN) and organic polymers like Poly(vinylidene fluoride) (PVDF) and Methylammonium Lead Iodide ($MAPbI_3$).

### 2.2.1. $ABO_3$

Among all the ferroelectrics, the inorganic ferroelectrics with genetic composition of $ABO_3$ are the most studied and most widely applied. Library of $ABO_3$ perovskite contains compounds like PZT, PT and BTO, as shown in Figure 10(a).[102, 103, 104] These $ABO_3$ ferroelectrics could be further divided into lead-containing and lead-free compounds. PZT is the dominating ferroelectric materials in the high-end commercial market for its remarkable ferroelectricity and mature ceramic fabrication process. Despite the high performance of devices with lead-containing materials, another group of lead-free oxides like BTO, BNT and BFO are attracting increasing attentions due to their environment-friendly feature and good ferroelectric properties.

A-site driven ferroelectric distortions is shown in Figure 10(b).[105] The ferroelectric domain

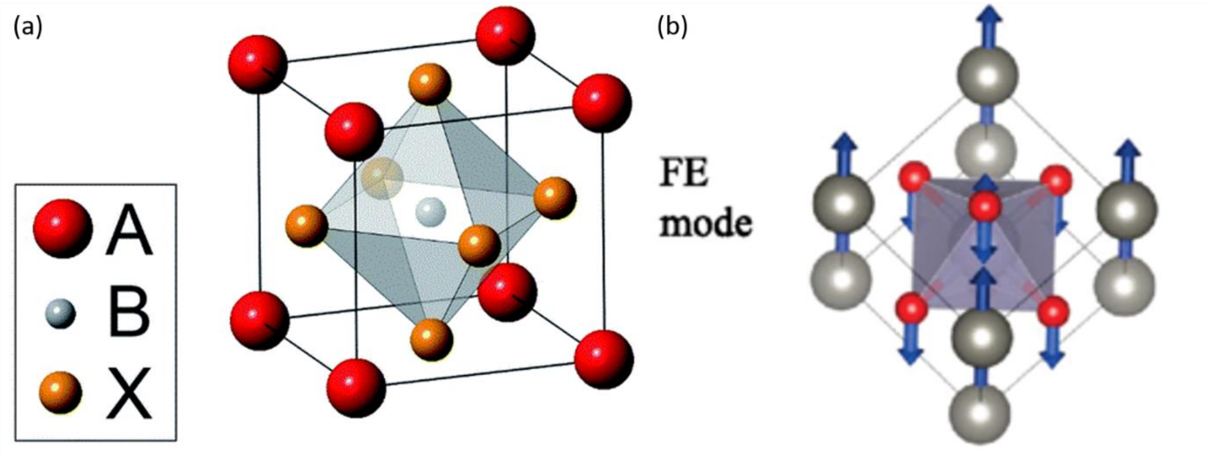

**Figure 10.** Structure of $ABO_3$ perovskite

strongly impacts the ferroelectricity. Ferroelectric domain refers to a region where the polarization shares the same orientation without any external stimuli. That is to say, all the domain states have the same energy. Furthermore, if an external electric field was applied to the ferroelectric material, polarization tends to be aligned to the same orientation and the free energy would be weakened. Consequently, the permanent polarization could be achieved by applying a large enough external electric field. The most important characteristic of the ferroelectrics is the hysteresis loop, known as the fingerprint of the ferroelectricity, which reveals the non-linear relation between the polarization and external electric field. In addition, the direction of polarization could be reversed by switching the electric field. Different crystallographic forms (e.g. texture, polycrystalline and epitaxial) may significantly influence the material properties and their applications. For instance, the grain and grain boundaries have modulation effects on the polarization and other parameters.[106] Defects in the nano layer structure could lead to stress inside the material and, as well, impact the device performances.[107]

Other common methods to characterize the ferroelectricity of materials include the capacitance-voltage (C-V) characteristics, also known as the "butterfly curve", leakage current and fatigue measurements. Key parameters of ferroelectric materials include the dielectric constant, coercive field, remnant polarization etc. Figure 11 is the measurements of PZT layer. [108]

Most of the ferroelectrics have intrinsic large bandgap (see Table 2). Ferroelectric thin films possess optical properties including high transparency at visible band, high dielectric constant nonlinear optical response which are particularly useful in lasers for nonlinear optical frequency conversion. In ferroelectric materials, polarization depends on the electric field and incident light, which could be expressed as

$$\vec{P} = \varepsilon_0\chi^{(1)}\cdot\vec{E}+\varepsilon_0\chi^{(2)}:\vec{E}\vec{E}+\varepsilon_0\chi^{(3)}\vdots\vec{E}\vec{E}\vec{E}+\cdots = P^{(1)}+P^{NL}$$

where the first term is the linear optical property of with $\chi^{(1)}$. The $\chi^{(2)}$ and $\chi^{(3)}$, are the

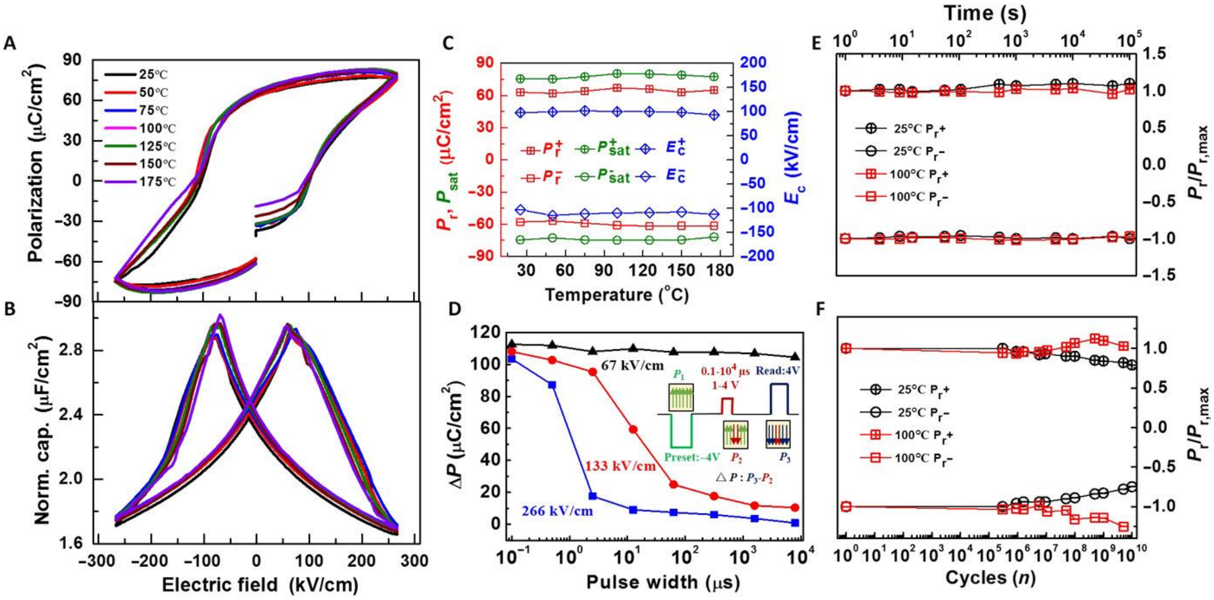

**Figure 11.** Electrical properties of PZT thin film. (a)*P*-*E* and (b)*C*-*E* hysteresis loops at various temperatures. (c) Remnant, saturation polarizations, and coercive field as functions of temperature. (d) PUND switching polarization as a function of pulse width at different voltages. The inset shows the measurement sequence. Retention (e) and fatigue (f) measurements at two typical temperatures second- and third-order nonlinear optical susceptibilities, which correspond to nonlinear optical properties of the material. The second order nonlinearity could induce the sum- and difference-frequency generation, Raman scattering, Brillouin scattering and optical parametric oscillation (OPO) etc. For the third

**Table 2.** Bandgap of the typical ferroelectrics

| Ferroelectrics | Band gap (eV) | Reference |
|---|---|---|
| PZT (Pure) | 3.4-4.0 | [169, 170, 171] |
| PZT (Doped) | 2.74-3.10 | [169] |
| BTO | 2.6 | [172] |
| R‘ BFO | 2.65-2.82 | [173, 174] |
| T‘ BFO | 3.1 | [173] |
| HZO | bulk | [175][175] |

order nonlinearity of the material, phase conjugation, four-wave mixing and nonlinear absorption could be observed.

Polarization of the domains could be modulated by the external optical field. [2, 109] Incident light interacts with ferroelectrics generally in two ways. One is the thermal induced polarization reverse. The incident light with high energy intensity illuminating on the ferroelectrics, which results in continuous increase of temperature in local ferroelectrics and eventually induces polarization switches.[110, 111] It is noticed that such thermal induced polarization switch is irreversible. The other method for light induced polarization switch is based on the open circuit voltage generated from the ferroelectrics, which is also known as bulk photovoltaic (BPV) effect.[112] Li *et al.* has reported the polarization switch by BPV effect in $BiFeO_3$.[113] With light on the surface of ferroelectrics, equilibrium carriers were generated and thus induce photo current $I_{ph}$ in the layer. A build-in electric field was established along the direction of photo current which is, equivalently, considered as a current source. If the build-in electric field could be raise to values higher than the coercive field, polarization of the ferroelectrics can be switched. It is worth mentioning that the polarization is reversible with incident light illuminating on different regions. Moreover, controlling of the strong laser field, tip-enhancement of the light as well as tuning illumination area could also achieve reversible ferroelectric polarization switching, as shown in Figure 12. [114]

### 2.2.2. Ferroelectric Polymers

Moreover, organic ferroelectric polymers have also been studied due to their good mechanical property and flexibility. The organic ferroelectric materials are represented by PVDF and its derives. PVDF is one of the most studied material. There are four typical lattice structure in PVDF including α, β, γ and δ phase, which is also known as the I, II, III and IV phases. Structure of PVDF-TrFE was shown in Figure 13. The α-PVDF forms into orthorhombic cell with two chains packing in opposite directions resulting in canceling of the dipole moments, which consequently makes the α-phase PVDF non-polar and paraelectric. β-PVDF shares o-phase as well yet the structure of the lattice is in all-trans planar zigzag conformation with fluorine atoms on one side. β-PVDF could thus achieve the highest dipole moment and

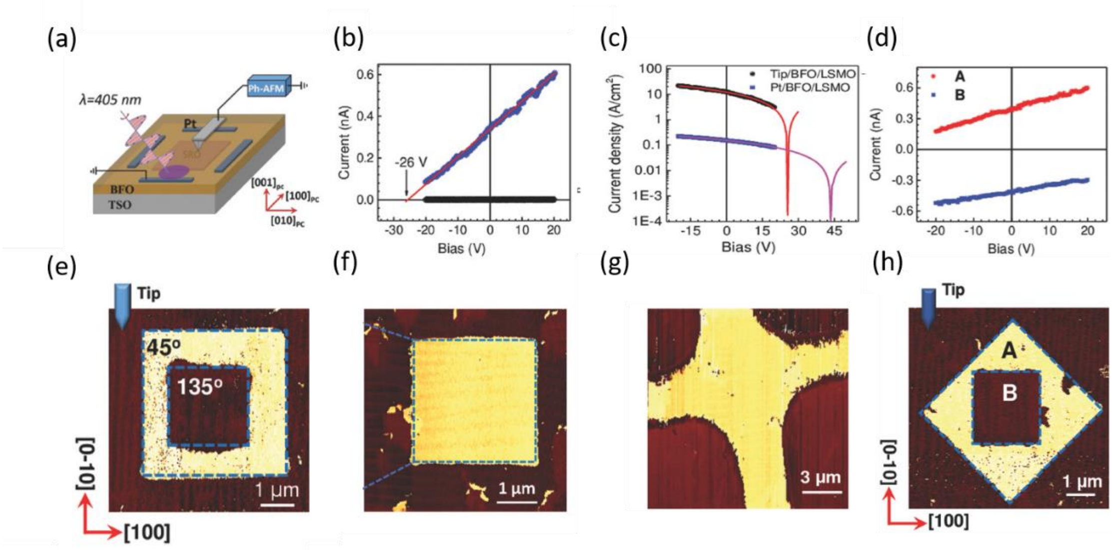

**Figure 12.** Various methods for the light induced polarization in ferroelectric BFO layer. (a) Schematic illustration of the device and the light incidence. (e) is polarization switching generated from the polarized incident light. (b) is Local current-voltage characteristics with and without illumination at tip-enhancement method and (f) is the corresponding PFM result. (c) is the current density-voltage dependence of tip/BFO/SRO and the Pt/BFO/SRO capacitors and (g) is the PFM amplitude which demonstrated polarization switching with illumination as a result of photocurrent density. (d) and (h) are the polarization switching via tuning illumination.

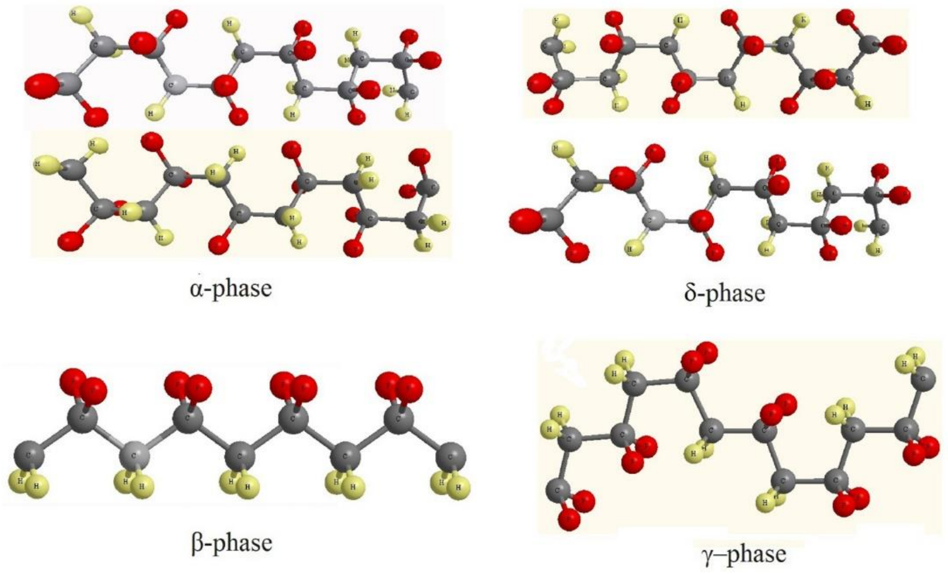

α-phase δ-phase β-phase γ–phase

**Figure 13.** Structure of PVDF crystalline.

become the most popular structure of PVDF with the best ferroelectricity and piezoelectricity among all the phases. Crystalline PVDF with γ-phase is monoclinic with partial dipole moment, which also show ferroelectricity. The δ-phase structure resembles the α-phase but with the second chain rotating 180° along the chain axis. Such structure could result in the polar behavior and show ferroelectric property. P(VDF-TrFE) polymer is composed of PVDF and TrFE, which is of the most popular ferroelectric polymers among the PVDF based materials.

Incident photons with high energy like X-ray could generate defects in P(VDF-TrFE) and free carriers generated have impact on the reversal of polarization. It was reported that with X-ray illuminating on the polarized P(VDF-TrFE) films, a clear phase difference of 180° as well as domain boundaries was observed. The loss in ferroelectricity will significantly reduce the poled domain area with X-ray irradiation and the domains would be rarely poled after illumination for 60 minutes. [115]

### 2.3. 2D materials/Ferroelectrics hybrid system

Compared to 2D materials on $SiO_2$/Si substrates, suspended counterparts $MoS_2$ has enhanced conductivity. However, if one changes the supporting substrates from $SiO_2$/Si to other functional ones, the properties of 2D materials and thus related device performances could be effectively modulated. In addition to holding the 2D materials, these functional substrates play an important part in mechanical, chemical, electronic and optoelectronic properties of the 2D nanosheets. Defects and impurity at the interface as well as the lattice mismatch between the $MoS_2$ and substrate could all impact the structure of the nanosheets. Then the related charge transfer, interface strain, dielectric screening effect, as well as the optical interference in the 2D semiconductor subsequently impact the device performances.

### 2.3.1. Electrical interaction of 2D/ferroelectrics hybrid system

Polarization switching in ferroelectrics has been proved to be able to establish a build-in electric field in 2D materials, which could further modulate the electrical properties of the 2D materials.

Therefore, FETs combining 2D materials and ferroelectric layers has been investigated. One of the most typical phenomena observed in the early studies was that the clock-wise hysteresis loop in the transfer property of FET devices, as shown in Figure 14.[116] This hysteresis loop was believed to be originated from adsorbents of water molecules rather than ferroelectric

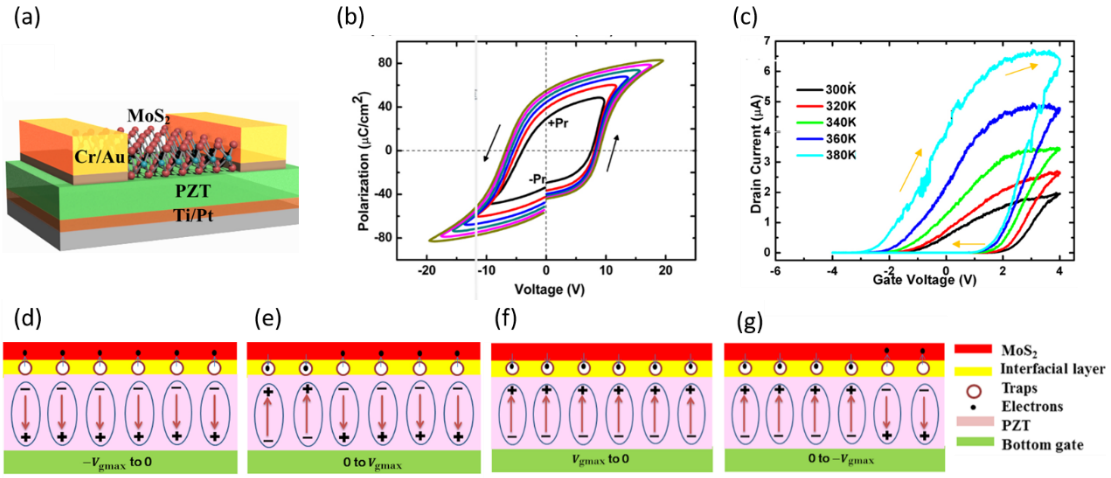

**Figure 14.** Hysteresis behaviors induced by the interfacial states of $MoS_2$/PZT FETs. (a) is the devices structure. (b) is the polarization-voltage characterization of PZT film and (c) is the transfer characteristics of the device with anti-hysteresis loop. (d)-(g) is the physical mechanism of charge trapping and de-trapping at the interface of $MoS_2$/PZT hybrid system.

polarization switching which should induce anti-clockwise loop [153,154]. Such clockwise hysteresis was also observed in other 2D materials/ ferroelectrics hybrid system. In addition to water molecules absorbents, other possible reasons like oxide charge trapping and surface charge trapping are also discussed. [117, 118] Hysteresis in ferroelectric devices have undermined the reliability of the devices and scientists have dedicated to solve this issue. Jang et al. has proposed a probable method to eliminate the hysteresis generated from charge trapping in the ferroelectrics. [119] In the devices contain ferroelectric layer, two hysteresis loops with opposite direction exist which is the loop induced by ionic migration in 2D ferroelectrics and loop induced by charge trapping, respectively. These two negative effects might neutralize with each other by modulating the activation energy for ionic migration in

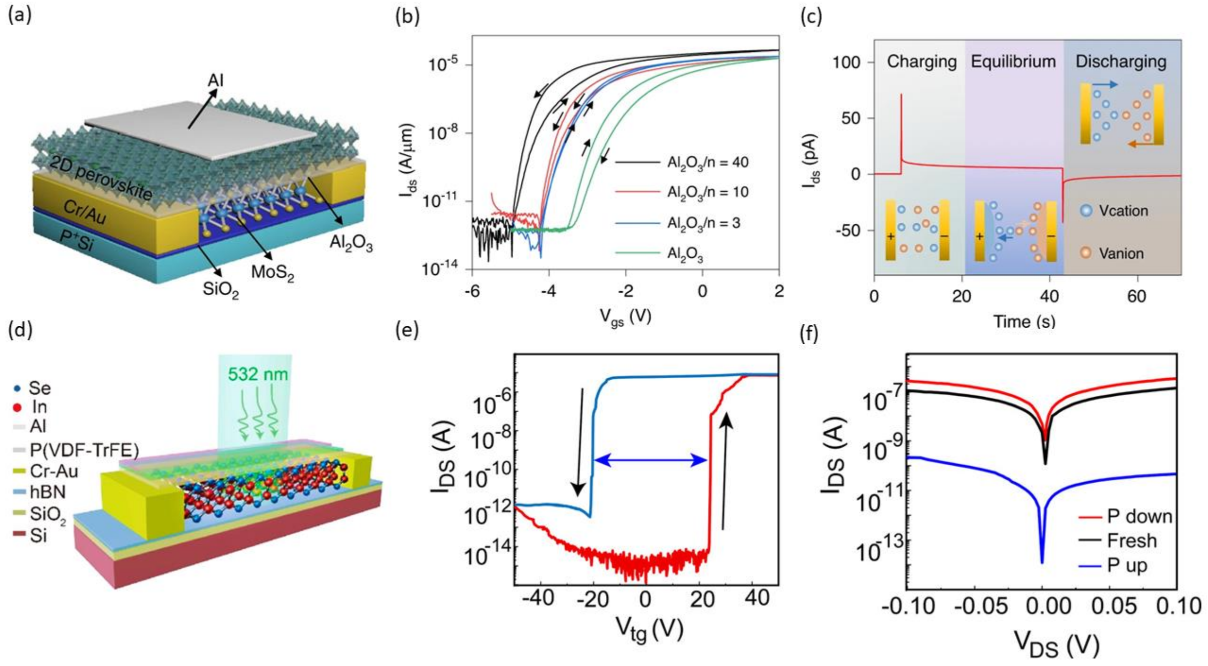

**Figure 15.** (a) $MoS_2$ phototransistor with $Al_2O_3$/2D perovskite heterostructure dielectric. (b) Transfer characteristics of the devices. The neglectable hysteresis loop is achieved. (c) is the schematic illustration of charging-discharging process. (d) is the device structure of InSe photodetectors gated by P(VDF-TrFE). (e) is the anti-clockwise memory window achieved with bias voltage switching from -40 V to 40 V and (f) is the output characteristics of the InSe FET with different polarization states.

ferroelectrics, see in Figure 15(a). These rectified devices have proved excellent rectifying characteristics and high performance in photodetection. [120] InSe photodetectors gated by ferroelectrics (shown in Figure 15(b)) has reported anti-clockwise hysteresis in the experiments, as shown in Figure 15(c).

Despite the charge trapping induced clockwise hysteresis, the hysteresis generated ferroelectrics could also be observed in the devices as shown in Figure 15 (d). Anti-clockwise memory window was observed with bias applied from -40 V to 40 V, shown in Figure 15 (e) and the electrical properties varied with different polarization states, see Figure 15 (f).

In addition to the hysteresis observed in 2D materials and ferroelectrics hybrid system. The dielectric screening effect is capable of modulating the electron-electron interactions as well in the layer adjacent to the substrate, leading to band structures variation and Fermi level shift. Moreover, the electronic transport of 2D materials could be tuned by ferroelectrics with

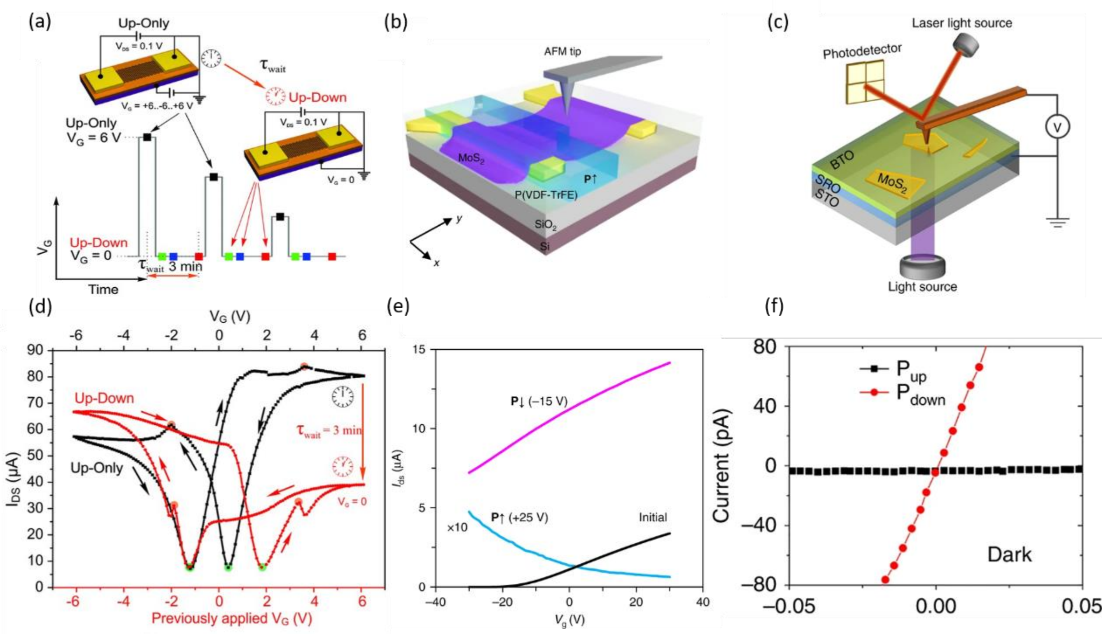

**Figure 16.** Electrical properties of the devices modulate by ferroelectric polarization. (a) and (d) are demonstrated the hysteresis reversal in graphene-PZT FeFETs and the $I_{ds}$-$V_{gs}$ voltage of +25V and down poling voltage of -15V.[122] (c) and (f) demonstrated the polarization induced dark current variation in the $MoS_2$/BTO FETs.[113]

polarized-up and -down were measured.[121] (b) and (e) is the is the $I_{ds}$-$V_{gs}$ characteristics of MoS2 FETs with PVDF as ferroelectrics and polarized by up poling polarization, as shown in Figure 16.[121, 122, 113] For example, the carrier type of the 2D materials could be modulated by the ferroelectric polarization switching. [123] Reversal of the polarization of the underneath ferroelectric film has led to the conversion of graphene from p-type to n-type, resulting in the reversible switching of the resistance in graphene. Similar results has been achieved by other researches with different 2D materials like $MoS_2$, $MoTe_2$ and InSe.[122, 45, 120] Low-voltage operation could be achieved with high-k ferroelectrics and the retention time of the devices could be improved [159].

2.3.2. Optoelectronic properties in 2D/ferroelectrics hybrid system

With 2D semiconductor in combination with ferroelectric layers, memory devices are capable of being written and erased both electrically and optically.[14] Moreover, ferroelectric films would be much easier to achieve polarization reversal than the pristine ferroelectrics with the assistance of 2D materials due to the compensation charge generated from 2D materials with incident light. As shown in Figure 17, $MoS_2$/BTO/SRO structure was fabricated and the

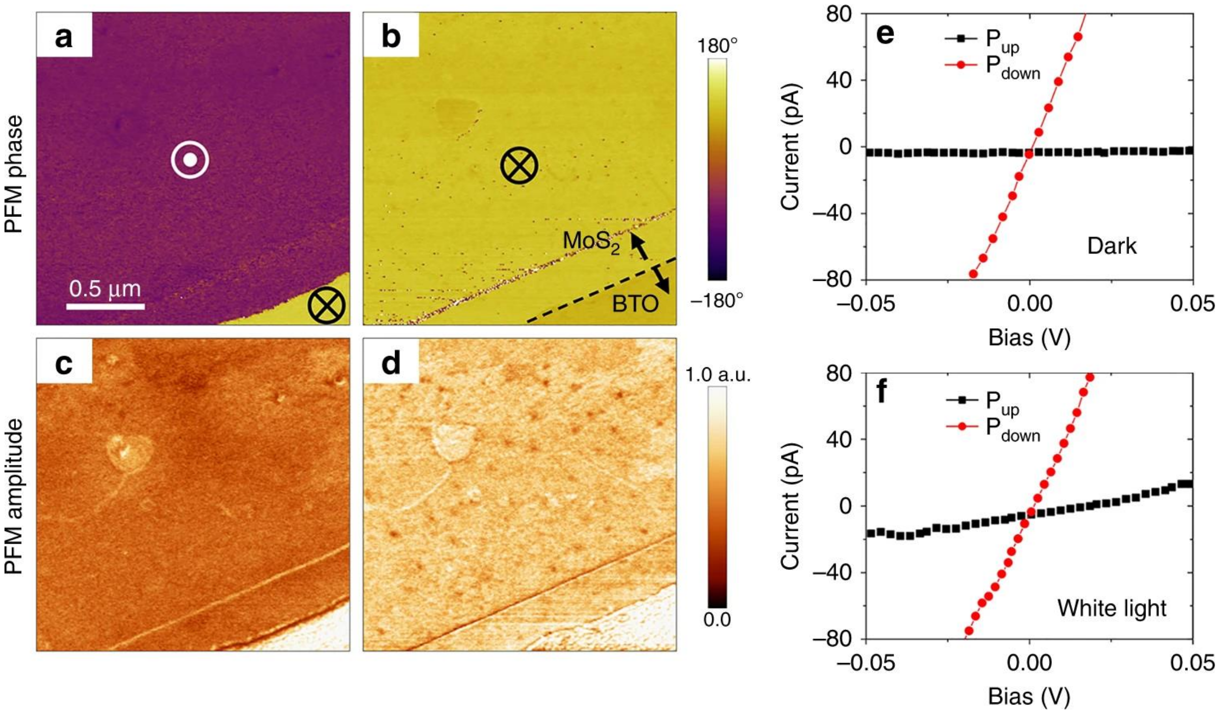

**Figure 17.** Polarization switching induced by external electric field. [124]

underneath BTO was able to be polarized by external electric field with $MoS_2$ on top. Ultra-violet (UV) light irradiation was then applied in the structure and optical induced polarization reversal was observed, as shown in Figure 17(b)-(e). The illumination of the structure leads to an accumulation of photon-generated carrier at the interface. Charge accumulation could modulate the built electric field and consequently change the electric field applied on the BTO, resulting in polarization switching in the BTO layer.[124] Polarization could also be modulated by the intensity of incident light and the piezo-response microscopy (PFM) amplitude signal, which varied because the photon-induced carriers devoted to the modulation of the electric field at the interface. Similar X-ray induced polarization has been studied with different ferroelectrics. [115]

In addition to photon induced polarization reversal with assistance of 2D materials, the impact on optoelectronic properties of 2D materials caused by ferroelectrics has also been observed.

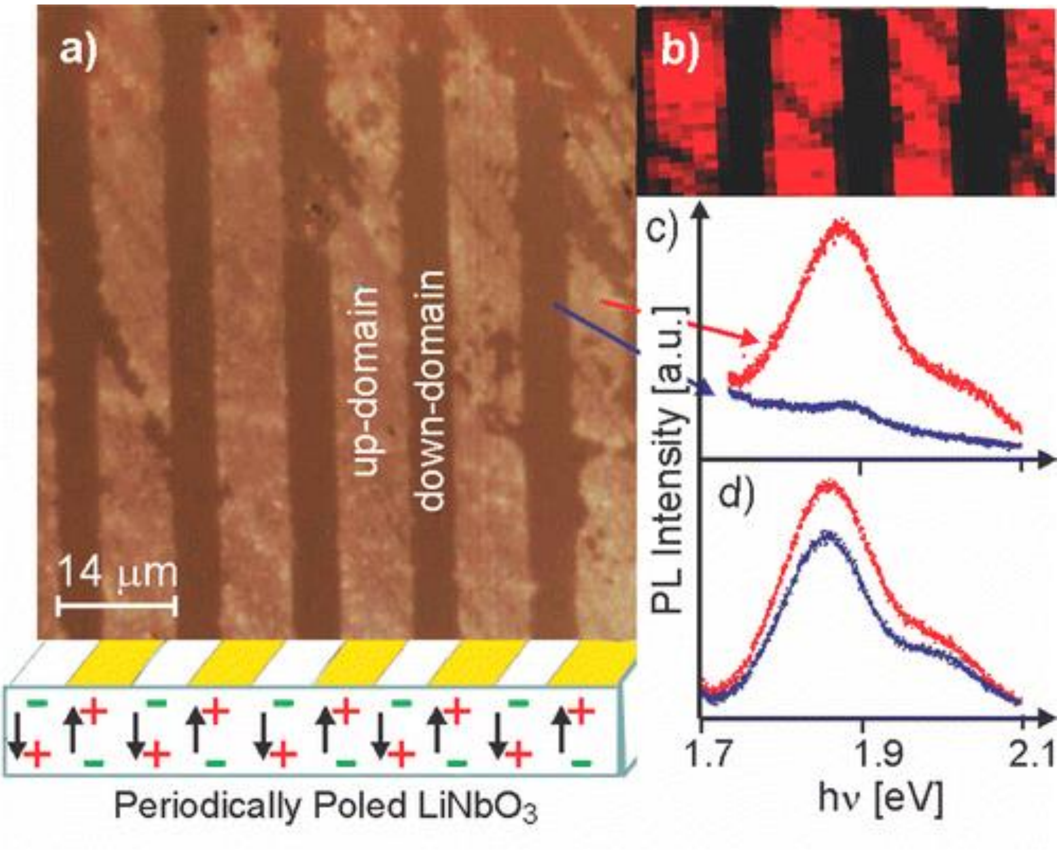

**Figure 18.** Optical microscopy of selective deposited MoS2 on pre-polarized LN and the photoluminescence of the $MoS_2$ island. [125]

$LiNbO_3$ (LN) is a ferroelectric material widely applied in optical devices thanks to its outstanding nonlinear optical properties. LN could be pre-polarized and applied as substrates for 2D materials. [125] $MoS_2$ was deposited on the periodically poled LN substrate. Selective growth of the $MoS_2$ was observed where enhance deposition of $MoS_2$ was found on the polarization “up” domain compared to polarization “down” domain. Optical properties of the deposited $MoS_2$ are influenced by the polarized LN, as illustrated in Figure 18. Polarization of the LN substrate could not only influence the growth but also the carrier transport of the $MoS_2$ overlayer.

Chemical vapor deposition (CVD) fabrication of $MoS_2$ requires high temperature of over 600℃, which is higher than the Curie temperature of many ferroelectrics and leads to the loss of polarization. Therefore, an alternative method, namely mechanical transfer for the realization of $MoS_2$ on ferroelectrics has been developed. [126] For instance, CVD grown $WS_2$ monolayer was mechanically transferred to a pre-polarized ferroelectric substrate and photoluminescence (PL) characterization of the $WS_2$ was measured. The spatial variation of

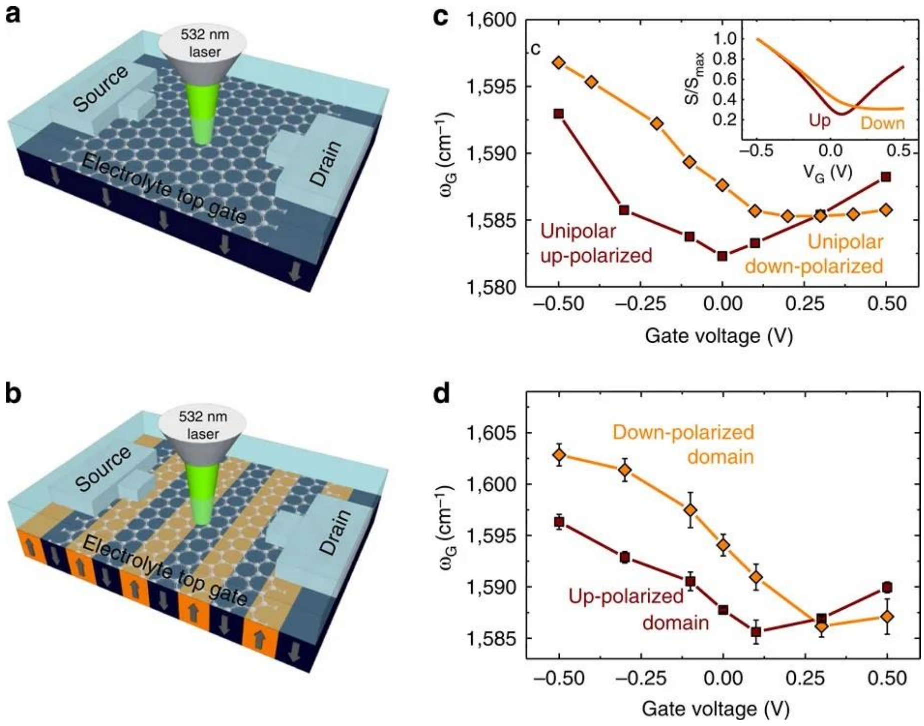

**Figure 19.** Ferroelectrically driven carrier density modulation in graphene

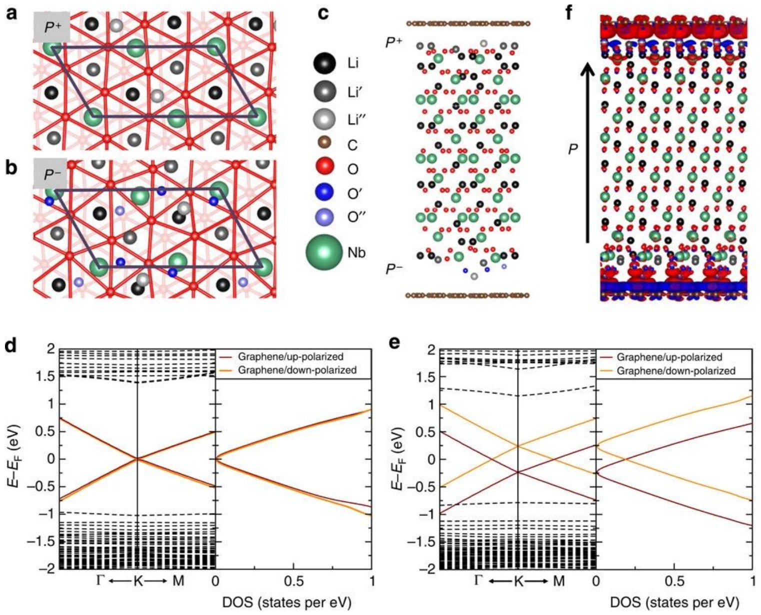

**Figure 20.** Theoretical study of the ferroelectrically control of carrier density in graphene with first-principle DFT.

PL spectra indicates the effective modulation of $WS_2$ monolayer by ferroelectric polarization. [126]

Photo-induced polarization in 2D/ferroelectrics hybrid structure has been proved to be dependent on the intensity of incident light. The ferroelectrics could also drive spatial carrier density modulation in the 2D materials of the hybrid structure,[127] as shown in Figure 19 reported by Baeumer *et al.* Characteristic peaks of Raman spectra shift in different polarization domain of the LN crystal. Two orders of magnitude carrier density difference were observed, which could origin from the graphene/LN interfacial chemistry effects. The interaction has also been theoretically calculated by the first-principle density-functional theory (DFT) calculations, as shown in Figure 20. Structure of the interface was constructed and the polarization was applied, as shown Figure 20(f). Calculation of the carrier density in graphene revealed that symmetrical charge densities in graphene was $6.75\times10^{12}$.

## 3. Photodetectors based on 2D materials and 2D materials/ferroelectrics hybrid system

### 3.1. Fundamentals of photodetection

2D materials with their superior photonic and optoelectronic properties has been extensively studied in nano devices. The TMDs nanosheets are a typical group material among the large amount and types of the 2D materials. The TMDs could be primarily considered as semiconductors with direct or indirect bandgap. Therefore, the principle and understanding of conventional semiconductor photodetection could be transferred to TMDs photodetection. The incident light generates carriers in semiconductors and they are then transported to electrodes. It is noticed that the signal amplification is sometimes applied in this procedure particularly in photodetectors due to the requirement of weak signal detection. Photodetection mechanism mainly consist of the photoconductive effect and photovoltaic effect. There are three main device structures for semiconductor photodetectors, the PN junction and related devices, Schottky junctions and field effect transistors.

Semiconductors could absorb the illuminated light and transfer photons to signals like voltage or current. This photodetection process could occur only when the incident photons possess larger energy than the bandgap of semiconductor materials, i.e.

$$\hbar v \geq \hbar v_0 = E_g \quad (1)$$

where the $\hbar v_0$ is the threshold energy that enables the intrinsic absorption. Moreover, for semiconductors with the indirect bandgap, the probability of the transition is much smaller than that of direct transitions, due to the participation of the phonons. Other absorption including exciton absorption, free carrier absorption and impurity absorption. During the photodetection, electrons in the valence band transit to the conductive band under illumination and generate extra electrons and holes, leading to signals of current or voltage. Photo-generated current could be expressed as

$$I_c = q\eta \frac{P}{hv} \quad (2)$$

Consider $A = \frac{q\eta}{hv}$ is the proportionality constant, which represents the sensitivity of the photodetector.

Mechanism of photodetection mainly includes the photoconductive and the photovoltaic ones. The conductivity increases of semiconductors due to light illumination has been briefly introduced before (see section 2.3), which is known as the photoconductive effect, as shown in Figure 21.

The generation rate of the photogenerated carriers is proportional to incident light intensity. The photogenerated carriers constantly generate and recombination, the density of photon-generated carriers is

$$\Delta n_0 = \Delta p_0 = g\tau \quad (3)$$

where g is the generation rate of photogenerated carriers, τ is the average carrier life-time. Consider the incident light power of P, g could be written as

$$g = \eta \frac{P}{hvAL} \quad (4)$$

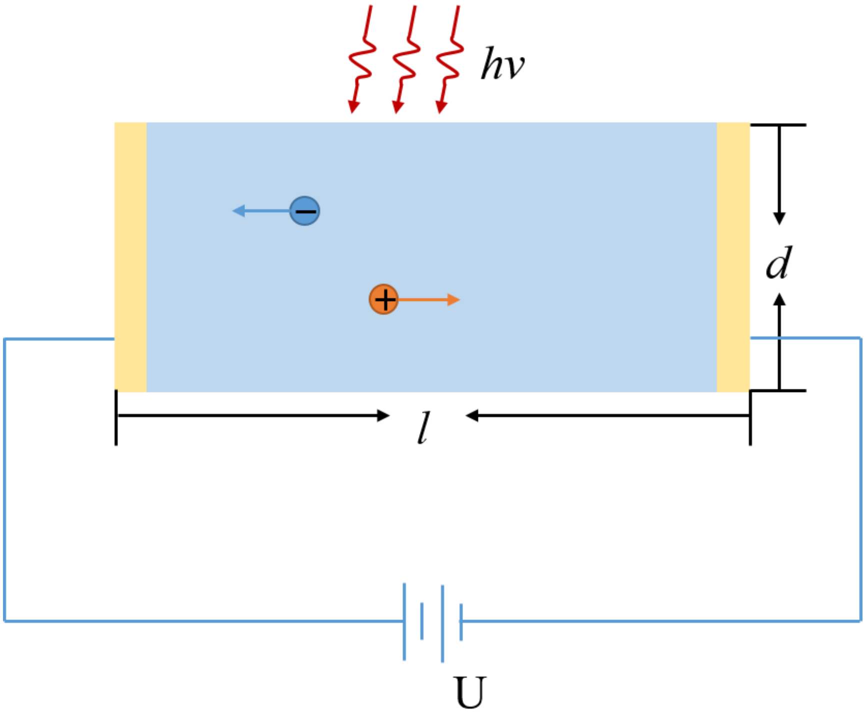

**Figure 21.** Basic principle of photoconductive current generation

where η is the quantum efficiency, A and L is the cross-section area and the length of the material, respectively. Short-circuit photocurrent density with external electric field is

$$\Delta J_0 = E \cdot \Delta\sigma = q\tau\eta\left(\mu_n + \mu_p\right)\frac{P}{hvAL}E \quad (5)$$

Electrical conductivity and photocurrent both increase as the intensity of illumination augments. Photocurrent is then:

$$I_p = \frac{U\Delta\sigma A}{L} = \frac{qUA\left(\Delta n\mu_n + \Delta p\mu_p\right)}{L} = \frac{qNU}{L^2}\left(\Delta n\mu_n + \Delta p\mu_p\right) \quad (6)$$

where N is the number of generated electron-hole pairs; $\tau_n$ and $\tau_p$ are corresponding life-time of electrons and holes generated, respectively.

With illumination on the inhomogeneous semiconductor, the build-in electric field is formed and photo-generated current is observed when the circuit is shorted. Such optoelectronic effect is photo-voltaic effect.

Based on photoconductive and photovoltaic mechanism, different devices are developed, in which photoconductors and photodiodes are two typical representatives. Photoconductors are based on photoconductivity. Photo-conductors usually has wide band response, relatively high operating current and high sensitivity. With the incident light, the non-equilibrium carriers increase and consequently improve the conductivity of the materials, and the resistance is thus reduced under illumination.[128, 129] The photoconductive effect is sensitive to the nanostructure as well as the doping and defects of the semiconductors. Photoresistors based on 2D materials with wide band responsivity has been widely studied and reported by researchers. [130] It was demonstrated that the 2D materials are able to cover the UV to infra-red band with high responsivity and ultrasensitive properties.

Photodiodes are based on the photo-voltaic effect, which is also known as barrier-type photodetectors. Photodiodes include PN junction, the PIN junction, heterostructure and Schottky diodes.

Compared to photoconductors which require external voltage, photodiodes have certain polarities and thus the signals could be transferred without external voltage. Photodiodes also show fast responsivity and good frequency response.

Taking PN junction as an example to explain the photodetection process, the barrier region in a PN junction shares relatively strong build in electric field (from n-region point to p-region). Photo-generated carriers move in opposite directions under the build-in electric field. The electrons in p-region move to the n-region while the holes enter the p-region. Such movement of the electrons and holes consequently lead to potential reduction in the n-region and rise in the p-region. Electromotive force (EMF) across the PN junction generated with illumination results into a pressure drop $qV_D - qV$ and forward current $I_F$ .In addition to the photoresistor and PN diode, another group of devices enable photodetection could are as well studied profoundly, known as the phototransistors.

### 3.2. Figures of merit in photodetection

The most important parameters for photodetection are identified as speed, responsivity and sensitivity. Other parameters including quantum efficiency, noise and gain are important figures of merit as well. It is noted that here we only consider the semiconductor photodetector to understand the operation of the semiconductor photodetector and figures of merit for photodetection which are of vital importance to the materials parameters, device structure and performance. Definitions of the parameters of quantum efficiency, responsivity, sensitivity, response speed and photo gain are as follows:

“Quantum efficiency” could be divided into internal and external quantum efficiency, which are the most important parameters for semiconductor optoelectronic photodetectors. The internal quantum efficiency (IQE) is define as the number of electron-hole pairs generated by absorbing one incident photon, which is

$$IQE = 1 - e^{-\alpha(\lambda)W} \quad (7)$$

where $\alpha(\lambda)$ is the absorption coefficient of corresponding wavelength $\lambda$, W is the thickness of the absorption layer. It is demonstrated that the IQE increases with the absorption coefficient or the thickness of the absorption layer grows. In practical applications, there is no way for photons reach the absorption layer through the surface of the materials. Photons go through a heavily doped contact area with photon loss rather than passing through the surface of materials to reach the absorption layer. Simultaneously, the reflection of the surface also consumes part of the incident photons. Thus, the external quantum efficiency (EQE) is defined as

$$\begin{aligned} EQE &= \left(1-R_f\right)e^{-\alpha(\lambda)d}\cdot IQE \\ &= \frac{I_p/q}{P/hv} \end{aligned} \qquad (8)$$

where $d$ is the thickness of contact area and $R_f$ is the surface reflectivity on photodetector.

“Responsivity” of a photodetector is the voltage or current of photodetector output divided by the input power, which could be categorized into spectral responsivity ($R_\lambda$) and integral responsivity ($R$). If the photo-induced current ($I_{ph}$) is measured with incident power of P,

$$R = \frac{I_{ph}}{P} \quad (9)$$

according to the definition of quantum efficiency, then

$$R = EQE\cdot\frac{q}{hv} \quad (10)$$

where $q$ is the electronic charge.

“Sensitivity” of a photodetector is the minimum photon signal detected under certain transmission bandwidth and rate. It measures the photoelectric conversion characteristics, as well as the spectral and frequency conversion characteristics.

"Response speed" of photodiode is evaluated by the rise/fall time ($\tau_r/\tau_f$) of the detective signal. The response speed is defined as the frequency where the photocurrent decreases to $1/\sqrt{2}$ from peak in frequency domain. Incident photons will go into the semiconductor through the surface layer, then photo-generated carriers and free electron-hole pairs shift under the electric field. The time required for incident photons to be transferred to photocurrent is the "response time". Three main factors could affect the response time, including the diffusion and transition time in the depletion region, as well as the RC time constant of the photodiode.

The "noise equivalent power (NEP)" is another key parameter for photodetection, which refers to the input signal power which results in a signal-to-noise ratio (S/R) of 1 in a 1 Hz output bandwidth. [131]NEP has expressed the sensitivity of photodetectors. Another typical parameter being correlated to the NEP is the "detectivity" ($D^*$).

$$D^* = \frac{(A \cdot \Delta f)^{\frac{1}{2}}}{NEP} \quad (11)$$

where, $A$ is the area of the photosensitive region and the $\Delta f$ is the frequency bandwidth of the detector.

"Photogain" is a benchmarked parameter for photoconductive detectors, which is

$$G_{ph} = (I_{ph}/q)/(\Phi_{in} QE) \quad (12)$$

where $\Phi_{in} = \frac{P}{hv}$ is the incoming photon flux. Here we bring another definition of External Quantum Efficiency (EQE) for sensitized photoconductors as $QE = \eta_{trans}\eta_{abs}$, where $\eta_{trans}$ is the charge transfer efficiency and $\eta_{abs}$ is the absorption efficiency, which demonstrates the number of detected charge carriers per single incident photon. The photogain can also been quantified by the ratio of the lifetime of the trapped carriers ($\tau_{life}$) over the drift transit time ($\tau_{transit}$). If we take a FET for example, a bias ($V_{bias}$) is applied to a FET device, the $G_{ph}$ can

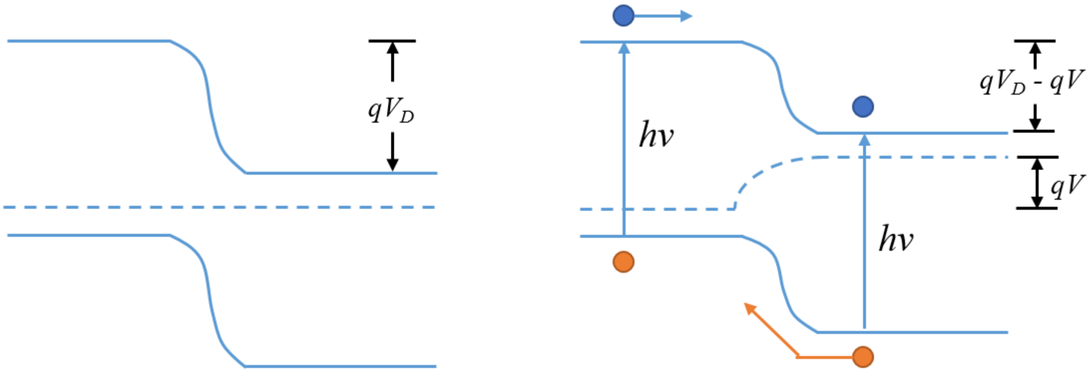

**Figure 22.** Band structure of PN junction and the mechanism of photodetection.

be defined as

$$G_{ph} = \frac{\tau_{life} \cdot \mu \cdot V_{bias}}{L^2} \quad (13)$$

where $L$ is the channel length, $\mu$ is the carrier mobility.

### 3.3. Photodetectors based on PN junctions

For 2D materials, iron-doping and adsorbates of the materials are often applied to achieve p-type or n-type semiconductors, as shown in Figure 22. Structure of 2D materials applied in the devices are basically categorized into the homojunction and heterojunction. Detectors based on various 2D materials has been reported. [132] Graphene PN junction was formed by applying voltages with opposite polarities on the top and bottom gate, as shown in Figure 23(a)-(c). Thermo-induced carriers were considered to play an important role in the optoelectronic response of graphene, and the photocurrent was demonstrated to be >40 nA with a relatively low voltage bias and an incident light with the wavelength of 850 nm. Responsivity was correspondingly measured to be 5 mA $W^{-1}$ which was relatively small compared with FETs photodetectors, yet larger than the previously reported 1 mA $W^{-1}$. MoS2 homojunction photodetectors with a ultra-high responsivity of $7\times10^4$ A $W^{-1}$ and EQE>10% has been reported by Huo *et al*. [133] p-type and n-type $MoS_2$ was achieved by chemical doping and form a vertical junction as

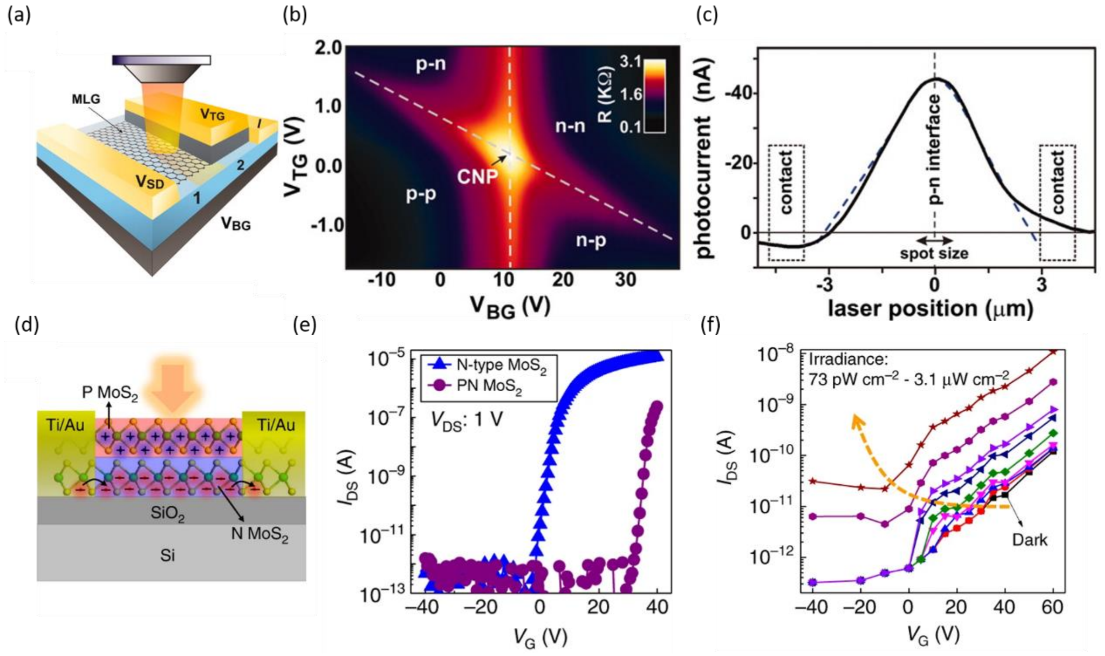

**Figure 23.** (a)-(c)Photodetectors based on graphene homo-junction and the photocurrent with incident light. (d)MoS2 homojunction photodetector, (e)electrical properties of the devices and (f) photocurrent generated with light illumination.

shown in Figure 24(d)-(f). Moreover, TMDs including $WSe_2$, $WS_2$, $MoTe_2$ et al. have been utilized in the photodetectors. [134] The photodetectors using 2D materials heterojunctions have also been investigated and optimized in many aspects, which are summarized in Ref. [135, 134, 136].

Lv et al. has also reported on the 2D photodetectors with $MoS_2$ homojunction. [122] Doping in $MoS_2$ channel was reconfigurable by ferroelectric polarization. Polarization upward of P(VDF-TrFE) with was applied as ferroelectric layer in the experiments due to its remarkable coercive field of ~$5\times10^7$ V $m^{-1}$. The $MoS_2$ channel turned into p-type semiconductor with upward polarization and reversal of external electric field resulted in switch of majority carriers, as n-type doping were enhanced in the $MoS_2$ channel. $10^9$-$10^{13}$ $cm^{-2}$ doping in $MoS_2$ was achieved by ferroelectric polarization. It is noticed that voltage applied in polarization process varies with different channel materials (eg. $|V_P|$<10V with $MoS_2$ and |Vp|=±6 V with $WSe_2$).As shown in Figure 24, responsivity of the photodetector has reached up to $10^2$.

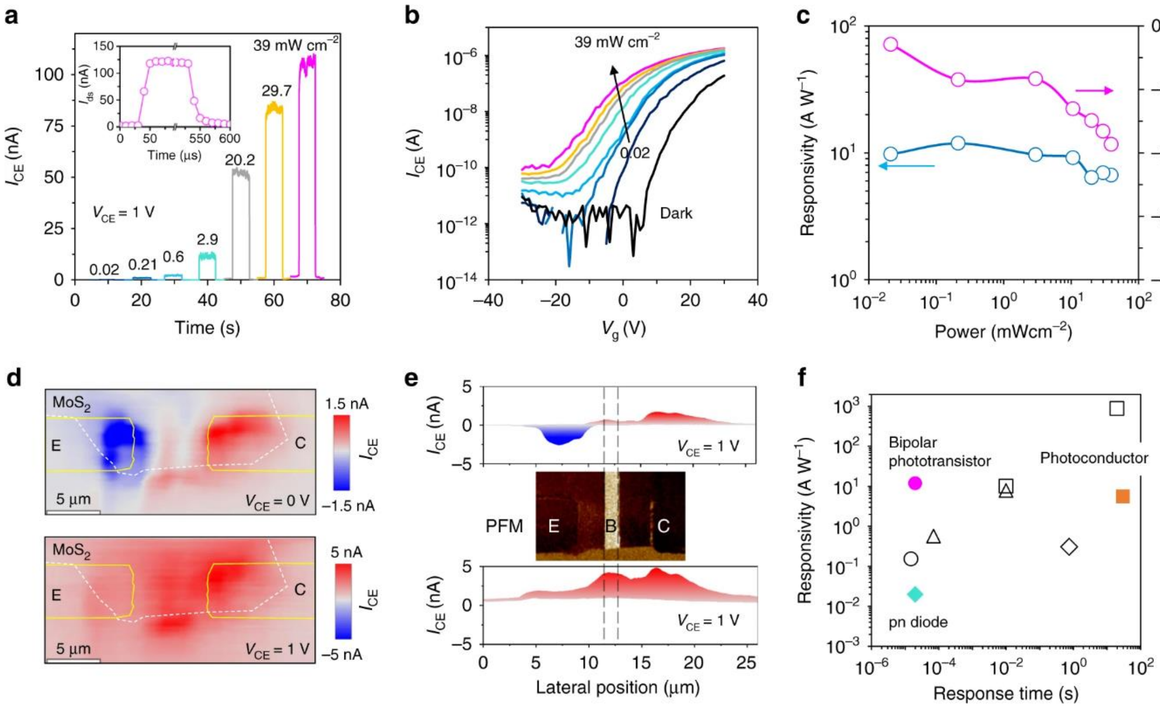

**Figure 24.** Performance of the MoS$_2$ homojunction photodetectors.

PN junctions based 2D-ferroelectrics hybrid structures are also studied, in which the polarization of ferroelectrics could induce carrier transport of 2D materials. Responsivity of the device was kept in the magnitude with UV spectrum, which confirmed the function of the photodetector at UV region. Moreover, ferroelectrics applied in the photodetector could effectively influence the device performance. [137]

In addition to the devices based on MoS$_2$ with ferroelectrics, similar researches have been carried out with various materials. Wu et al has reported MoTe$_2$ PN junction defined by ferroelectrics, as shown in Figure 25.[45] PN junction could be converted to n-p, n-n and p-p doping by external voltage pulses, as shown in Figure 25(b). Such modified photodetector under illumination of different wavelengths including 520 nm and infrared was investigated (see Figure 25(c) and Ref [45]). Other figures of merit including EQE and responsivity were studied as well and on/off ratio of $5\times10^5$ was achieved. The responsivity could reach 5 A W$^{-1}$, detectivity was $3\times10^{12}$ Jones as well as fast response time of 30 μs. Such PN junctions enable photodetection unveiled opportunities for advanced nano photodetectors and realizing next-generation optoelectronic devices.

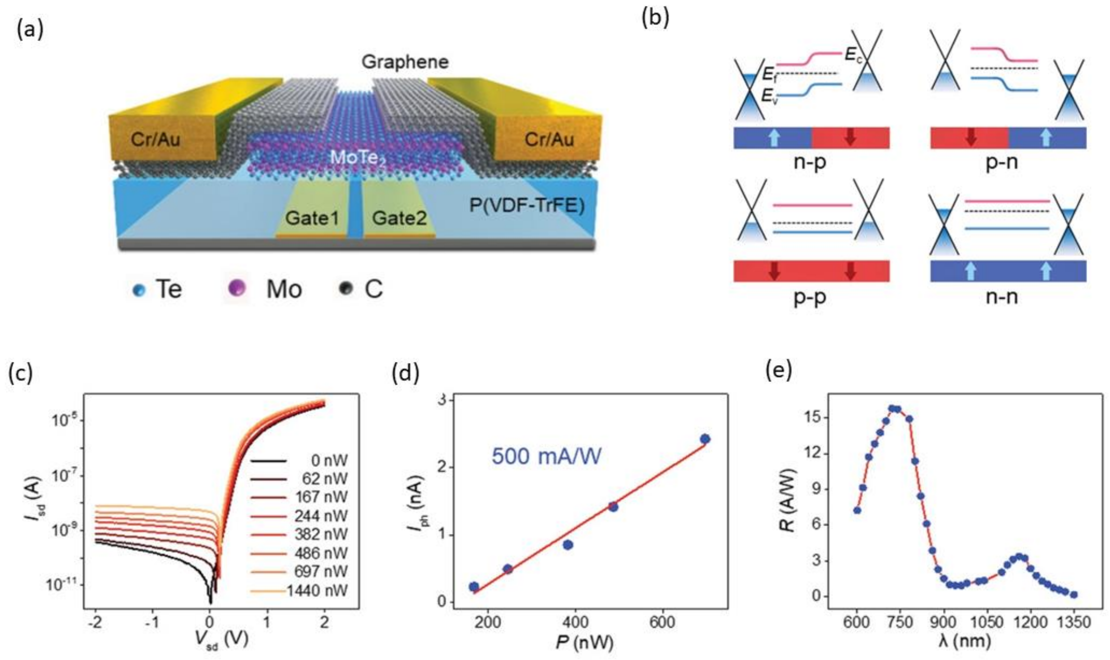

**Figure 25.** (a) MoTe2 PN junction controlled by ferroelectric domains. (b) switchable doping method defined by polarization. (c)-(e) are devices performances under different illumination.

### 3.4. Photodetectors based on field effect transistors

Photodetectors based on 2D materials FETs with monolayer graphene as the channel were reported in 2008 for the first time. [138] Zero-bandgap graphene has the advantages of wide band response, which allows facile generation of photocurrent by the incident light. Photocurrent of the graphene photodetector with 514.5 nm incident light reached a maximum of ~350 nA with the gate bias varied in a relatively large range (-40 V-40 V), and the photocurrent modulation by the gate bias was obviously observed in the devices, as shown in Figure 26(a)-(c). Suspended graphene monolayer has high Fermi velocity (~1/300 of the speed of light in vacuum) and huge electrical mobility (200,000 $cm^2V^{-1}s^{-1}$). Photocurrent of the graphene FETs photodetectors has reached over 1 μA and the maximal responsivity was 0.5 mA $W^{-1}$. [28] For optical communication, the photoresponse in communication band is a priority. Graphene has responsivity of 6.1 mA $W^{-1}$ at the wavelength of 1550 nm. Back gate monolayer graphene photodetectors at a data rate of 10 Gbit $s^{-1}$ at 1550 nm incident light was achieved, as shown in Figure 26(d)-(f).

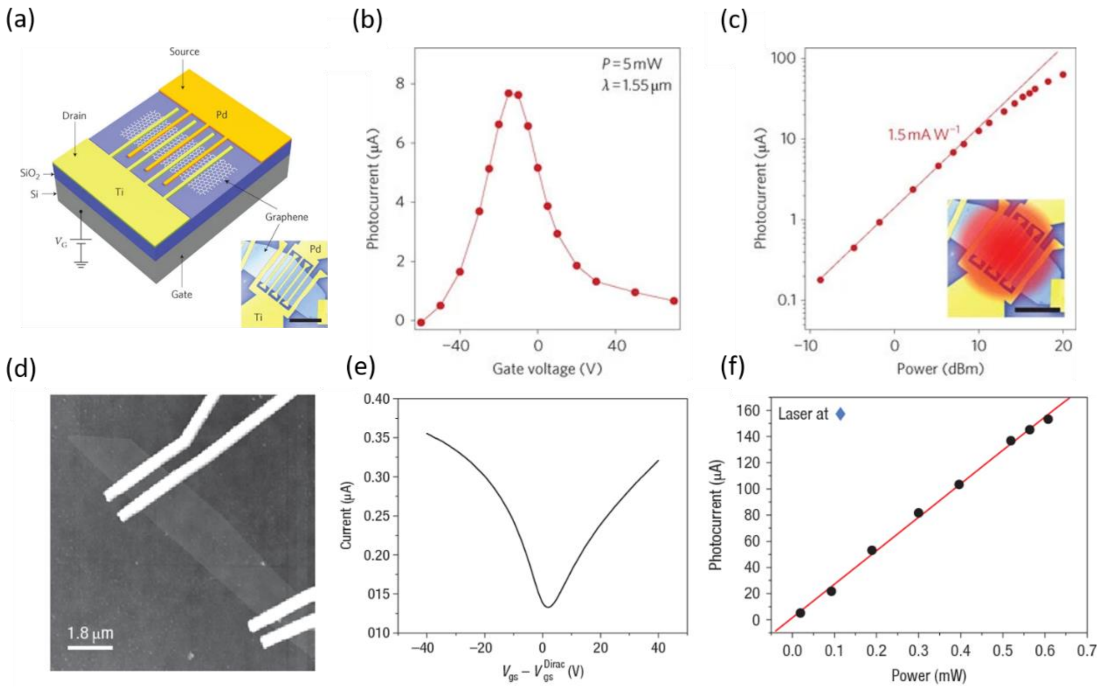

**Figure 26.** (a)-(c) is Graphene photodetectors where (a) is the structure of the devices, (b) and (c) are the photocurrent dependent on the gate voltage and incident power intensity, respectively.[138] (d)-(f) is Back gate monolayer graphene phototransistors enable high speed photo communication.[28]

Besides graphene other 2D materials, for instance the CNTs, TMDs and h-BN etc. have been also applied in photodetection inspired by graphene FETs photodetectors. Similar $MoS_2$ monolayer FET structures and devices have been reported, firstly by Yin et al. in 2011[129] One of the most prominent properties of the $MoS_2$ different from graphene is that monolayer $MoS_2$ has an intrinsic bandgap of 1.8 eV, which enables $MoS_2$ to be “switched off” in the FETs. However, the pristine $MoS_2$ has relatively low mobility ranging from 0.5 $cm^2V^{-1}s^{-1}$ to 3 $cm^2V^{-1}s^{-1}$, [139] which could result in the impurity scattering and remote charge. High-*k* dielectrics could be good in improving the transport properties which could provide charge screening and reduce the trap/impurity scattering, then could consequently improve the carrier mobility. Inorganic $HfO_2$ and $Al_2O_3$ are among the most studied dielectrics, for the organic materials, PVDF is a typical material that was utilized as the gate insulator. The mobility of $MoS_2$ could be increased by two orders of magnitude, together with high on/off ratio of $10^8$

and is thus very promising in the device applications [140]. In $MoS_2$ FET photodetectors, photocurrent is linearly proportional to the power of incident light High on/off ratio with ~$10^8$ could be achieved by high-k dielectrics like PZT, $HfO_2$ and $Al_2O_3$. On/off ratio for the simple back gate monolayer $MoS_2$ with $SiO_2$ as gate insulator was measured to be $10^2$-$10^3$, and the delay was at ~50 ms. [129] The back gate monolayer $MoS_2$ FET was fabricated and the photoresponsivity was 7.5 mA/W with low power incident light (P=80 μW) and medium gate bias ($V_g$=50 V) [129].

FET Photodetectors based on TMDs, BP and h-BN with remarkable photoresponse has also been studied and shown. Improvement of the devices performance and novel phenomena were found and discussed. 2D material heterostructures was achieved to realize the photodetection [141]. More recently, many studies are devoting themselves to realize flexible and transparent photodetectors using 2D materials, which are of great interest for the future applications of wearable and solar-energy devices.

Photodetectors based on 2D materials modulated by ferroelectrics has been reported since 2015. Initially ferroelectrics were introduced to 2D FET photodetectors only thanks to their high-k property, which can be used to enhance the photodetection performance. Wang *et al.* are among the first groups demonstrating $MoS_2$ based 2D photodetectors driven by ferroelectric P(PVDF-TrFE) and they proposed the device structure as shown in in Figure 27.[142] Few layer $MoS_2$ was used as semiconducting channel while the P(VDF-TrFE) was employed as the gate insulator. Dark current with non-polarized P(VDF-TrFE) was measured at $10^{-7}$-$10^{-8}$ A and could be depressed to <$10^{-10}$ A with polarized-up P(VDF-TrFE). Signal-to-noise-ratio reached $10^3$ using polarized gate. Illuminated by an incident light with a wavelength of 635 nm, the photocurrent of the device reached >50 μA at a low power of 1nW and 5 V source-drain voltage. Meanwhile, the stable polarization of P(VDF-TrFE) provided a high electric field (~$10^9$ V $m^{-1}$ within the nanometer scale) thus keeping the $MoS_2$ channel in the fully depleted state, which significantly improved the sensitivity of the detector. The

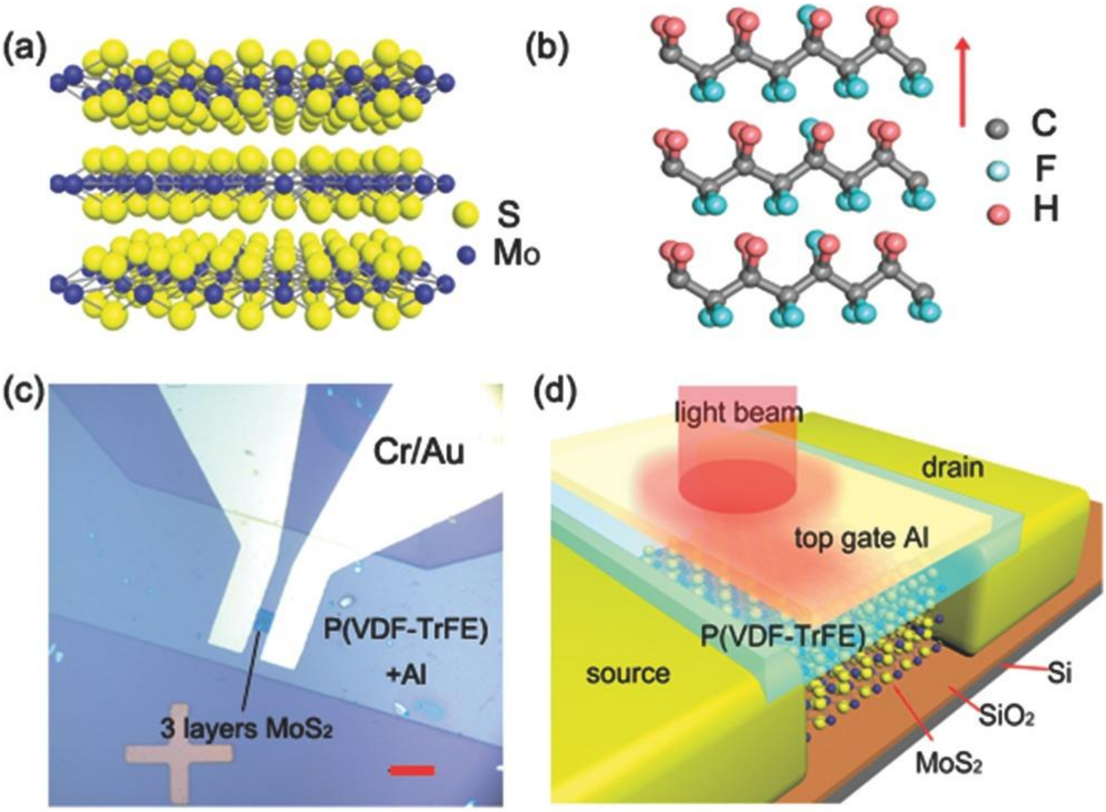

**Figure 27.** Ultra-sensitive $MoS_2$ photodetectors with ferroelectrics

photodetector reached quite a high detectivity ~$2.2\times10^{12}$ Jones and a responsivity up to 2570 A $W^{-1}$.

Similar 2D-ferroelectrics phototransistors have recently been extensively studied and reported. Wide band photodetection (from visible light to 1550 nm) was achieved and the relative high sensitivity >340 A $W^{-1}$ was measured with an incident light wavelength of 450nm.[143] Considering that both the crystalline structure of ferroelectric gate materials and the carrier transport fluctuation in the 2D materials strongly depend on the temperature variation, the temperature dependence of the 2D-ferroelectrics hybrid FET photodetectors have been studied. Chen *et al.* has reported that a low temperature of 200 K could transform the lattice structure of P(VDF-TrFE-CFE) into ferroelectrics/relaxor, which changes the property of P(VDF-TrFE) and could further modulate the band structure of the few-layer

$MoS_2$ material, enabling the long wavelength detection to 1550 nm, as shown in Figure 28.[143] Screening coulomb impurities of ferroelectrics could also enhance the carrier mobility of $MoS_2$.

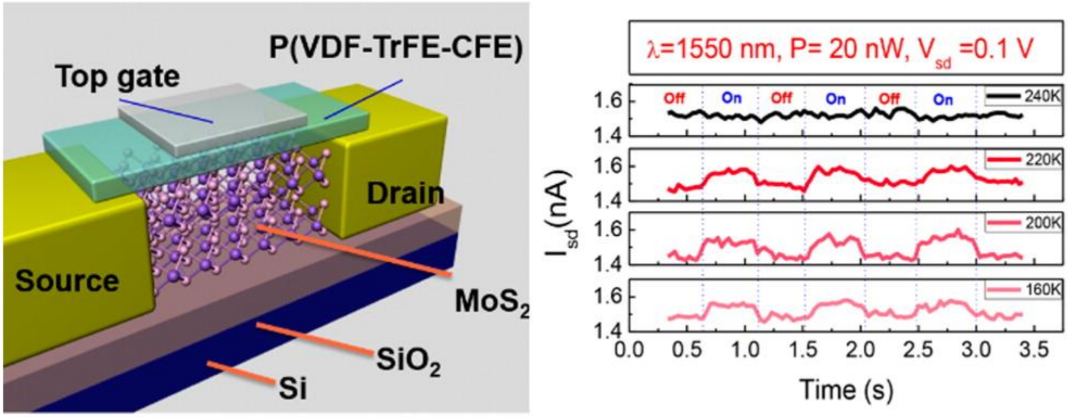

**Figure 28.** Schematic illustration of the $MoS_2$ photodetectors driven by ferroelectric gate and the temperature dependence of the response at 1550 nm incident light.

On-off ratio and delay are another two key figures of merits of the 2D-ferroelectrics hybrid photodetectors. On/off ratio of the devices was determined at zero gate bias at a low drain currents, while delay time of the devices accounts for the time required to switch the device on. Both on/off ratio and delay time express the response speed of the devices. On/off ratio for the monolayer $MoS_2$ based nano electronic devices could reach up to $10^8$ [144]and the simplest back gate FETs as photodetectors have an on/off ratio of $10^2$-$10^3$[145]. Application of the ferroelectrics has been proved to be able to significantly improve the sensitivity, the on/off ratio and the SNR of photodetector. On/off ratio of $MoS_2$ photodetector with P(VDF-TrFE) applied as ferroelectric gate was increased to $>10^4$ with dark current approximately to $10^{-11}$ A [146].

In the 2D-ferroelectrics hybrid photodetectors, some unique properties of 2D materials, like the plasmonic behaviors of graphene, could be modulated by the ferroelectrics, which further improve the photodetection performances. An ultra-high responsivity up to $7.62\times10^6$ A $W^{-1}$ has been reported graphene-ferroelectrics photodetectors, which is much beyond the previously reported experimental results. Meanwhile, detectivity reached $\sim 6.24\times10^7$ Jones with infra-red band photodetection. [147] Graphene was transferred on the pre-polarized ferroelectric substrate and the graphene plasmons was excited by the polarized domains. Graphene plasmons resonates at the boundaries, as shown in Figure 29. Polarized domains at the substrate could modulate the carrier density and the chemical potential (namely the Fermi level) of graphene by the external electric field. Broad band photodetector with wavelengths ranging from 5μm to20μm was achieved, as shown in Figure 30.

For the extensive investigation of 2D materials and ferroelectrics. There is a group of unique 2D semiconductors, represented by $\alpha$-In$_2$Se$_3$, shares both semiconductor property and the ferroelectricity. The combined properties make it potential in the ultra-thin photodetectors due to its capability of playing a dual role in the application of photodetectors. Hou et al has reported the $\alpha$-In$_2$Se$_3$ applied in the photodetectors, as shown in Figure 31. [148] Polarization of $\alpha$-In$_2$Se$_3$ pull the electrons to the surface of the materials and consequently forms into an electric field, which would influence the electrical properties of the photodetectors. On/off ratio of the photodetector was measured to be $2\times10^7$ and the comparison of the photodetector with and without polarization demonstrated that the polarization could prolong the decay yet significantly improve the on/off ratio with even three orders of magnitude, and

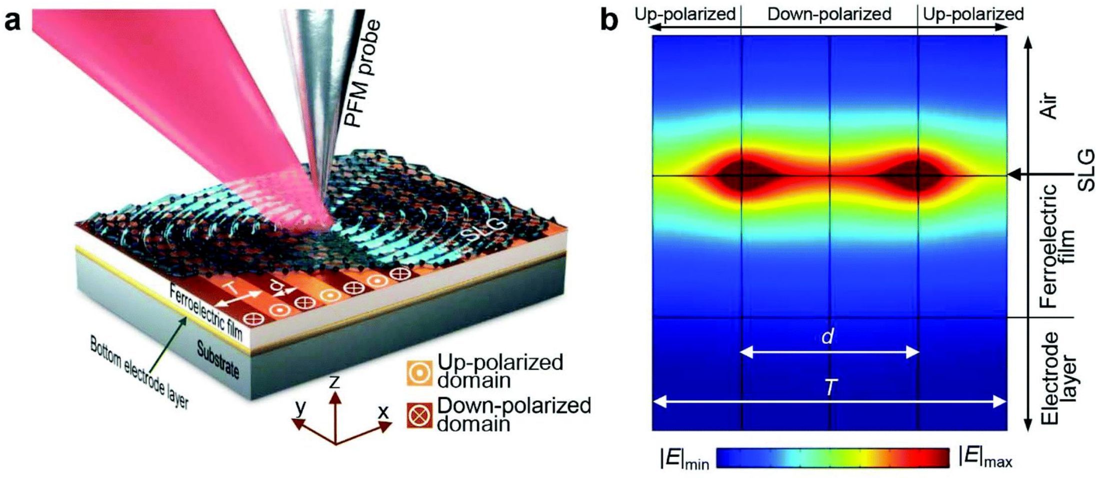

**Figure 29.** pre-polarized graphene photodetector and the plasmons excited by the polarized-up and -down domains

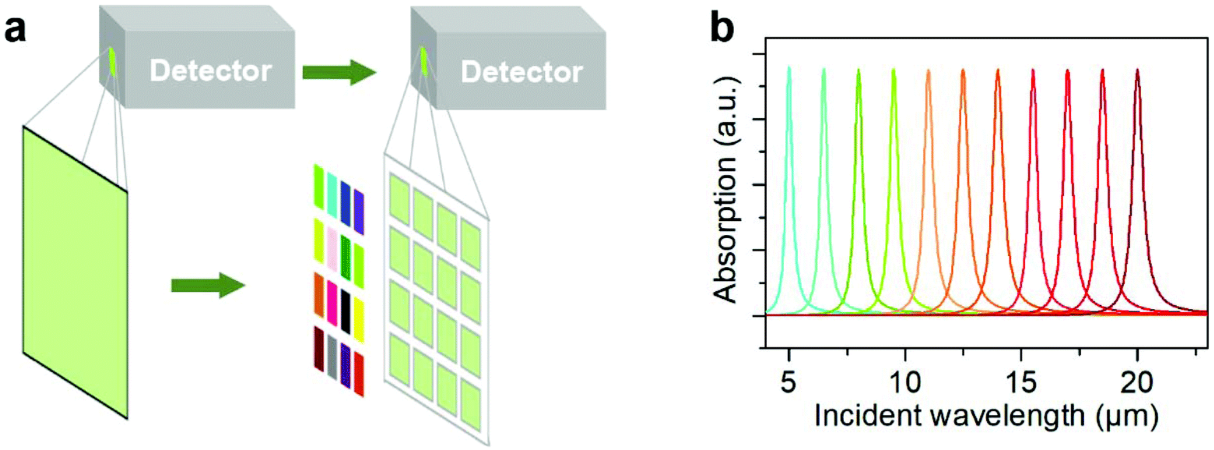

**Figure 30.** Graphene plasmonic photodetector controlled by ferroelectric domains and the wide-band response

Photodetectors with Pt electrodes could further optimize the on/off ratio by four orders of magnitude.

In addition to traditional ferroelectrics, recent emerged ferroelectric semiconductors have also attracted many interests and have been applied into 2D-ferroelectris hybrid photodetectors. The ferroelectric TMD α-indium selenide ($In_2Se_3$) is one typical representative. Photodetectors based on $WSe_2$ and α- $In_2Se_3$ heterostructures have been reported in 2020. [149] and ultra-low dark current of $10^{-13}$ A was achieved, which is a remarkable result compared to photodetectors with the similar structure. Meanwhile, such device also has high on/off ratio exceeding $1.24 \times 10^5$ and photoresponse of 26 mA $W^{-1}$. Liu *et al.* has also reported InSe2 photodetectors with P(VDF-TrFE) ferroelectric gate. [120] Different polarization of

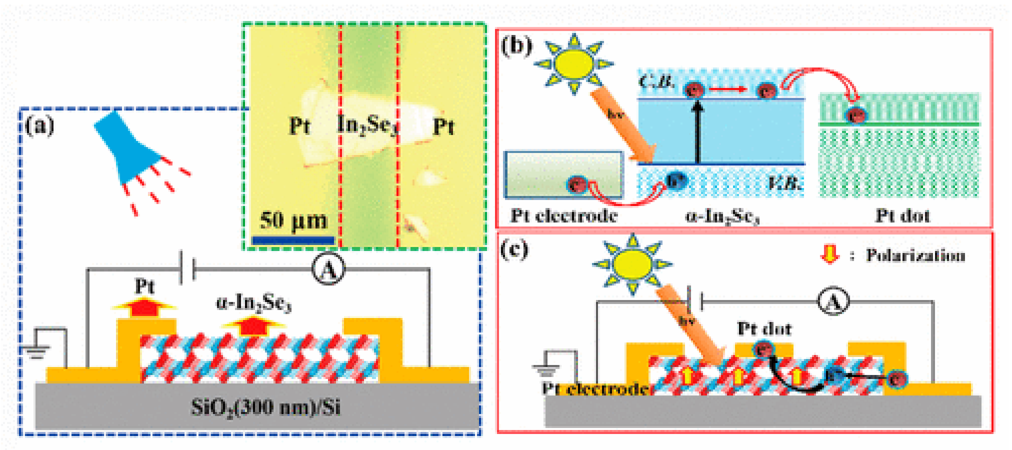

**Figure 31.** Schematics of the α-$In_2Se_3$ photodetector.

P(VDF-TrFE) was studied to improve the performance of the photodetector. High on/off ratio of $10^8$, fast response time of 600 μs and high photoresponsivity up to 14250 $AW^{-1}$ were achieved. However, few researches were focused on the ferroelectricity of InSe materials. Xu et al. as briefly reported the optoelectronic properties in $WSe_2/In_2Se_3$ heterostructures in 2018, $In_2Se_3$ was polarized and the output properties in dark and under illumination was investigated, as shown in Figure 32. Photocurrent was enhanced with positive voltage bias applied in gate dielectrics. Enhancement and weaken of the photocurrent were able to be modulated by varying the voltage bias from negative to positive, as shown in Figure 32(f). Photoresponse was thus improved by ferroelectric modulation.

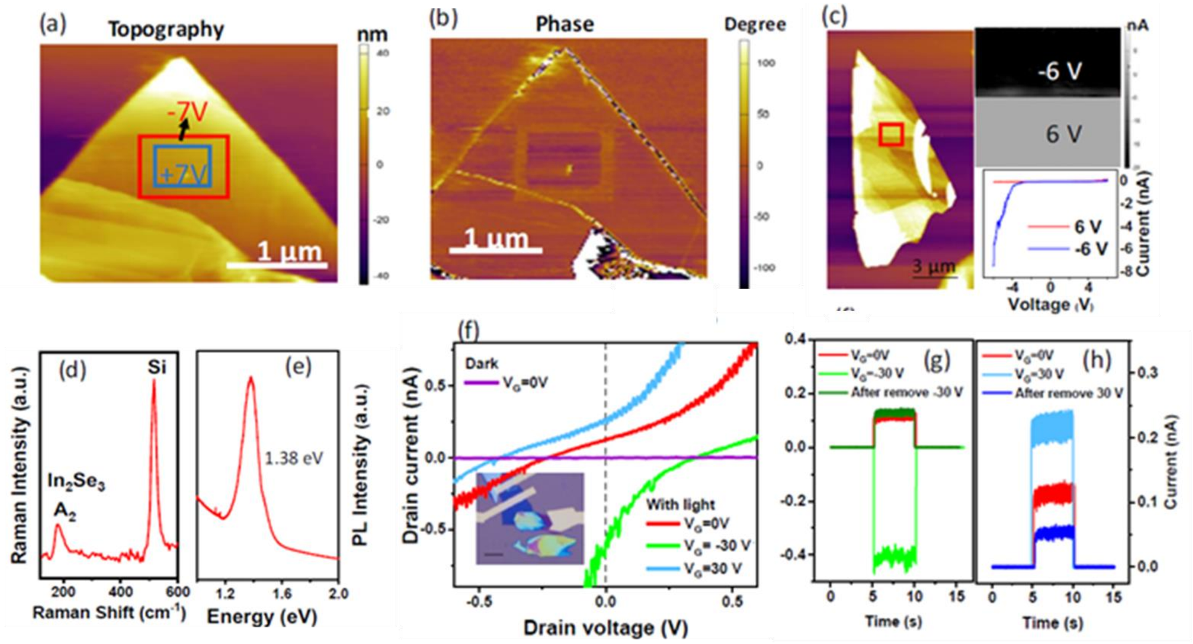

**Figure 32.** (a) Height image and (b) out-of-plane phase image of $In_2Se_3$ in PFM measurement. (c) Topography image, current mapping and local IV curves after writing with -6 V and 6 V in CAFM measurement. (d) Raman spectrum and (e) PL spectrum of a α-$In_2Se_3$ flake. (f) Photocurrent as a function of drain voltage of the photodetector based on $WSe_2/In_2Se_3$ heterostructure measured at various gate voltages. Inset: optical image of the device. (g) and (h) Short-circuit current as a function of time measured in a photodetector based on the $WSe_2/In_2Se_3$ heterostructure before, during, and after applied +30 V and -30 V gate voltages.

## 4. Conclusions and perspectives

In this review, we have reviewed the fundamentals of two-dimensional semiconductors and ferroelectrics as well as their application in photodetection. Hybrid system of two-dimensional materials and ferroelectrics could interact with each other, and thus realize higher performances and enable modulation of the devices. This novel combination structure has provided new methods for multiple functional nano-devices and compatible circuits.

In materials aspect, structure, physical properties, electrical properties as well as optoelectronic properties has been reviewed. Additionally, interaction between two-dimensional materials and ferroelectrics has been introduced.

In devices aspect, photodetectors based on two-dimensional materials and ferroelectrics has been categorized based on their structures and the performances as well as the interaction in the hybrid system has been reviewed. Researches based on two-dimensional materials and ferroelectrics have shown great potential in photodetectors. Remarkable achievements have witnessed however, problems still exit. Considering the structure of the devices, most of the researches focused on the field effect transistors with ferroelectrics as top gate, more work still remains to be done in the study of the ferroelectric layer applied as bottom gate as well as substrates. Meanwhile, photodetectors based on PN junctions are mostly based on the vertical heterojunctions with silicon as substrate or doped lateral junctions. Modulation of the carrier type and the junction generated from ferroelectric polarization has not been fully investigated either. Details and the mechanism of interaction between the two-dimensional semiconductor and the functional ferroelectric layer is still unintelligible, which is currently a challenge for the application of photodetectors based on 2D materials and ferroelectrics. As is mentioned before that the 2D materials has outstanding flexibility and mechanical strength, the joint ferroelectric substrates in the flexible devices are expecting to be flexible and transparent as well. Therefore, more attention is required on designing and fabrication of ultrathin ferroelectric film with high transparency and outstanding mechanical properties.

In conclusion, photodetectors based on two dimensional materials, ferroelectrics as well as the hybrid structures is promising structure for wide band high performance photodetection. Ferroelectric provide effective modulation of the devices and thus improve optical and optoelectronic properties of the devices. It is promising that the ferroelectric layer being applied as component of integrated circuit and will certainly lead to another prosperity area in exploring the road "More than Moore".

## Acknowledgements

We acknowledge the funding support from Key R&D Program of Shaanxi Province of China (2020GY-271 and 2018ZDXM-GY-150), the Fundamental Research Funds for the Central Universities(xjj2018016), the “111 Project” of China (B14040), the Open Project of State Key Laboratory of Infrared Technological Physic (Grant No. M201801), the Open Project of State Key Laboratory of Electronic Thin Films and Integrated Devices (KFJJ201902) and the Natural Sciences and Engineering Research Council of Canada (NSERC DG Grant No. 203773).

Received: ((will be filled in by the editorial staff))
Revised: ((will be filled in by the editorial staff))
Published online: ((will be filled in by the editorial staff))

## References

[1] L. Wang, X. Zou, J. Lin, J. Jiang, Y. Liu, X. Liu, X. Zhao, Y. F. Liu, J. C. Ho, L. Liao, *ACS Nano* **2019**, *13*, 4 4804.

[2] Z. Yang, L. Liao, F. Gong, F. Wang, Z. Wang, X. Liu, X. Xiao, W. Hu, J. He, X. Duan, *Nano Energy* **2018**, *49* 103 .

[3] A. D. Bartolomeo, G. Luongo, F. Giubileo, N. Funicello, G. Niu, T. Schroeder, M. Lisker, G. Lupina, *2D Materials* **2017**, *4*, 2 025075.

[4] C. Hu, D. Dong, X. Yang, K. Qiao, D. Yang, H. Deng, S. Yuan, J. Khan, Y. Lan, H. Song, J. Tang, *Advanced Functional Materials* **2017**, *27*, 2 1603605.

[5] F. Withers, O. Del Pozo-Zamudio, S. Schwarz, S. Dufferwiel, P. M. Walker, T. Godde, A. P. Rooney, A. Gholinia, C. R. Woods, P. Blake, S. J. Haigh, K. Watanabe, T. Taniguchi, I. L. Aleiner, A. K. Geim, V. I. Fal'ko, A. I. Tartakovskii, K. S. Novoselov, *Nano Lett.* **2015**, *15*, 12 8223.

[6] F. Withers, O. D. Pozo-Zamudio, A. Mishchenko, A. P. Rooney, A. Gholinia, K. Watanabe, T. Taniguchi, S. J. Haigh, A. K. Geim, A. I. Tartakovskii, K. S. Novoselov, *Nature Materials* **2015**, *14*, 3 301.

[7] O. Salehzadeh, M. Djavid, N. H. Tran, I. Shih, Z. Mi, *Nano Letters* **2015**, *15*, 8 5302.

[8] S. Riechel, C. Kallinger, U. Lemmer, J. Feldmann, A. Gombert, V. Wittwer, U. Scherf, *Applied Physics Letters* **2000**, *77*, 15 2310.

[9] G. Wu, X. Wang, P. Wang, H. Huang, Y. Chen, S. Sun, H. Shen, T. Lin, J. Wang, S. Zhang, L. Bian, J. Sun, X. Meng, J. Chu, *Nanotechnology* **2016**, *27*, 36 364002.

[10] L. Y. Rang, S. Wooseok, H. J. Kyu, L. Y. Bum, K. S. Jun, M. Sung, L. S. Sook, A. Ki-Seok, C. Chel-Jong, L. Jongsun, *Advanced Materials 28*, 25 5025.

[11] N. Huo, S. Gupta, G. Konstantatos, *Advanced Materials* **2017**, *29*, 17 1606576.

[12] K. S. Kim, Y. J. Ji, K. H. Kim, S. Choi, D.-H. Kang, K. Heo, S. Cho, S. Yim, S. Lee, J.-H. Park, Y. S. Jung, G. Y. Yeom, *Nature Communications* **2019**, *10*, 1 4701.

[13] E. O. Polat, G. Mercier, I. Nikitskiy, E. Puma, T. Galan, S. Gupta, M. Montagut, J. J. Piqueras, M. Bouwens, T. Durduran, G. Konstantatos, S. Goossens, F. Koppens, *Science Advances* **2019**, *5*, 9.

[14] A. Lipatov, P. Sharma, A. Gruverman, A. Sinitskii, *ACS Nano* **2015**, *9*, 8 8089.

[15] D. Xiang, T. Liu, J. Xu, J. Y. Tan, Z. Hu, B. Lei, Y. Zheng, J. Wu, A. H. C. Neto, L. Liu, W. Chen, *Nature Communications* **2018**, *9*, 1.

[16] M.-L. Tsai, S.-H. Su, J.-K. Chang, D.-S. Tsai, C.-H. Chen, C.-I. Wu, L.-J. Li, L.-J. Chen, J.-H. He, *ACS Nano* **2014**, *8*, 8 8317.

[17] Y. Tsuboi, F. Wang, D. Kozawa, K. Funahashi, S. Mouri, Y. Miyauchi, T. Takenobu, K. Matsuda, *Nanoscale* **2015**, *7*, 34 14476.

[18] T. Mueller, F. Xia, P. Avouris, *Nature Photonics* **2010**, *4* 297.

[19] Y. Tajima, B. Wrona, K. Mishima, *IEEE Transactions on Electron Devices* **1981**, *28*, 2 171.

[20] J.-P. Shim, S. K. Kim, H. Kim, G. Ju, H. Lim, S. Kim, H.-j. Kim, *APL Materials* **2018**, *6*, 1 016103.

[21] D.-H. Kwak, P. Ramasamy, Y.-S. Lee, M.-H. Jeong, J.-S. Lee, *ACS Appl. Mater. Interfaces* **2019**, *11*, 32 29041.

[22] A. Levi, M. Kirshner, O. Sinai, E. Peretz, O. Meshulam, A. Ghosh, N. Gotlib, C. Stern, S. Yuan, F. Xia, D. Naveh, *ACS Photonics* **2019**, *6*, 8 1910.

[23] C. Xu, Z. Du, Y. Huang, M. Dong, R. Lin, Y. Li, B. Wang, W. Zheng, F. Huang, *ACS Appl. Mater. Interfaces* **2018**, *10*, 49 42681.

[24] K.-J. Tielrooij, N. C. H. Hesp, A. Principi, M. B. Lundeberg, E. A. A. Pogna, L. Banszerus, Z. Mics, M. Massicotte, P. Schmidt, D. Davydovskaya, D. G. Purdie, I. Goykhman, G. Soavi, A. Lombardo, K. Watanabe, T. Taniguchi, M. Bonn, D. Turchinovich, C. Stampfer, A. C. Ferrari, G. Cerullo, M. Polini, F. H. L. Koppens, *Nature Nanotechnology* **2017**, *13*, 1 41.

[25] W. Zheng, R. Lin, J. Ran, Z. Zhang, X. Ji, F. Huang, *ACS Nano* **2018**, *12*, 1 425, pMID: 29298035.

[26] P. Ma, Y. Salamin, B. Baeuerle, A. Josten, W. Heni, A. Emboras, J. Leuthold, *ACS Photonics* **2019**, *6*, 1 154.

[27] K. S. Novoselov, A. K. Geim, S. V. Morozov, D. Jiang, Y. Zhang, S. V. Dubonos, I. V. Grigorieva, A. A. Firsov, *Science* **2004**, *306*, 5696 666.

[28] F. Xia, T. Mueller, Y. ming Lin, A. Valdes-Garcia, P. Avouris, *Nature Nanotechnology* **2009**, *4*, 12 839.

[29] H. Chang, H. Wu, *Advanced Functional Materials* **2012**, *23*, 16 1984.

[30] F. Bonaccorso, Z. Sun, T. Hasan, A. C. Ferrari, *Nature Photonics* **2010**, *4*, 9 611.

[31] Q. Bao, K. P. Loh, *ACS Nano* **2012**, *6*, 5 3677.

[32] H.-Y. Chiu, V. Perebeinos, Y.-M. Lin, P. Avouris, *Nano Letters* **2010**, *10*, 11 4634.

[33] S. Castilla, B. Terrés, M. Autore, L. Viti, J. Li, A. Y. Nikitin, I. Vangelidis, K. Watanabe, T. Taniguchi, E. Lidorikis, M. S. Vitiello, R. Hillenbrand, K.-J. Tielrooij, F. H. Koppens, *Nano Letters* **2019**, *19*, 5 2765.

[34] K. S. Novoselov, A. Mishchenko, A. Carvalho, A. H. C. Neto, *Science* **2016**, *353*, 6298 aac9439.

[35] A. Gupta, T. Sakthivel, S. Seal, *Progress in Materials Science* **2015**, *73* 44.

[36] X. Li, L. Tao, Z. Chen, H. Fang, X. Li, X. Wang, J.-B. Xu, H. Zhu, *Applied Physics Reviews* **2017**, *4*, 2 021306.

[37] X. Yao, Y. Wang, X. Lang, Y. Zhu, Q. Jiang, *Physica E: Low-dimensional Systems and Nanostructures* **2019**, *109* 11.

[38] X.-L. Li, W.-P. Han, J.-B. Wu, X.-F. Qiao, J. Zhang, P.-H. Tan, *Advanced Functional Materials* **2017**, *27*, 19 1604468.

[39] I. Husein, R. P. Jenie, In *Ferroelectrics and Their Applications*. InTech, **2018**.

[40] Y. Zhang, W. Jie, P. Chen, W. Liu, J. Hao, *Advanced Materials* **2018**, *30*, 34 1707007.

[41] L. Li, X. Liu, Y. Li, Z. Xu, Z. Wu, S. Han, K. Tao, M. Hong, J. Luo, Z. Sun, *Journal of the American Chemical Society* **2019**, *141*, 6 2623, pMID: 30661350.

[42] Y. Yuan, Z. Xiao, B. Yang, J. Huang, *J. Mater. Chem. A* **2014**, *2*, 17 6027.

[43] A. Lipatov, T. Li, N. S. Vorobeva, A. Sinitskii, A. Gruverman, *Nano Letters* **2019**, *19*, 5 3194.

[44] J. Íñiguez, P. Zubko, I. Luk'yanchuk, A. Cano, *Nature Reviews Materials* **2019**, *4*, 4 243.

[45] G. Wu, X. Wang, Y. Chen, S. Wu, B. Wu, Y. Jiang, H. Shen, T. Lin, Q. Liu, X. Wang, P. Zhou, S. Zhang, W. Hu, X. Meng, J. Chu, J. Wang, *Advanced Materials* **2020**, *32*, 16 1907937.

[46] C. A. Randall, D. J. Barber, R. W. Whatmore, *Journal of Materials Science* **1987**, *22*, 3 925.

[47] Z. Surowiak, M. Kupriyanov, D. Czekaj, *Journal of the European Ceramic Society* **2001**, *21*, 10-11 1377.

[48] K. Kushida-Abdelghafar, H. Miki, K. Torii, Y. Fujisaki, *Applied Physics Letters* **1996**, *69*, 21 3188.

[49] R. Moazzami, C. Hu, W. H. Shepherd, *IEEE Transactions on Electron Devices* **1992**, *39*, 9 2044.

[50] B. Ravel, E. A. Stern, R. I. Vedrinskii, V. Kraizman, *Ferroelectrics* **1998**, *206*, 1 407.

[51] C. Xiong, W. H. P. Pernice, J. H. Ngai, J. W. Reiner, D. Kumah, F. J. Walker, C. H. Ahn, H. X. Tang, *Nano Letters* **2014**, *14*, 3 1419.

[52] E. Strelcov, A. V. Ievlev, S. Jesse, I. I. Kravchenko, V. Y. Shur, S. V. Kalinin, *Advanced Materials* **2013**, *26*, 6 958.

[53] A. Kuroda, S. Kurimura, Y. Uesu, *Applied Physics Letters* **1996**, *69*, 11 1565.

[54] K. Y. Yun, M. Noda, M. Okuyama, *Applied Physics Letters* **2003**, *83*, 19 3981.

[55] T. Choi, S. Lee, Y. J. Choi, V. Kiryukhin, S.-W. Cheong, *Science* **2009**, *324*, 5923 63.

[56] G. D. Hu, S. H. Fan, C. H. Yang, W. B. Wu, *Applied Physics Letters* **2008**, *92*, 19 192905.

[57] S. Trolier-McKinstry, C. A. Randall, *Journal of the American Ceramic Society* **2017**, *100*, 8 3346.

[58] M. Sharma, G. Madras, S. Bose, *Physical Chemistry Chemical Physics* **2014**, *16*, 28 14792.

[59] S. Lee, Y. Lee, *Carbon* **2018**, *126* 176.

[60] W. Ren, Y. Fang, E. Wang, *ACS Nano* **2011**, *5*, 8 6425.

[61] D. A. Hon-Sum Philip Wong, *Carbon Nanotube and Graphene Device Physics*, Cambridge University Press, **2014**.

[62] S. Reich, J. Maultzsch, C. Thomsen, P. Ordejón, *Physical Review B* **2002**, *66*, 3.

[63] G. Gui, J. Li, J. Zhong, *Physical Review B* **2008**, *78*, 7.

[64] M. Gmitra, S. Konschuh, C. Ertler, C. Ambrosch-Draxl, J. Fabian, *Phys. Rev. B* **2009**, *80* 235431.

[65] J.-H. Chen, W. G. Cullen, C. Jang, M. S. Fuhrer, E. D. Williams, *Physical Review Letters* **2009**, *102*, 23.

[66] K. Bolotin, K. Sikes, Z. Jiang, M. Klima, G. Fudenberg, J. Hone, P. Kim, H. Stormer, *Solid State Communications* **2008**, *146*, 9-10 351.

[67] F. Schwierz, *Nature Nanotechnology* **2010**, *5*, 7 487.

[68] J. Yu, G. Liu, A. V. Sumant, V. Goyal, A. A. Balandin, *Nano Letters* **2012**, *12*, 3 1603.

[69] K. Zhao, T. Zhang, A. Ren, Y. Yang, P. Xiao, Z. Ge, Y. Ma, Y. Chen, *Carbon* **2019**, *141* 198.

[70] T. Yu, E.-K. Lee, B. Briggs, B. Nagabhirava, B. Yu, *IEEE Electron Device Letters* **2010**, *31*, 10 1155.

[71] A. A. Balandin, S. Ghosh, W. Bao, I. Calizo, D. Teweldebrhan, F. Miao, C. N. Lau, *Nano Letters* **2008**, *8*, 3 902.

[72] J. S. Moon, M. Antcliffe, H. C. Seo, D. Curtis, S. Lin, A. Schmitz, I. Milosavljevic, A. A. Kiselev, R. S. Ross, D. K. Gaskill, P. M. Campbell, R. C. Fitch, K.-M. Lee, P. Asbeck, *Applied Physics Letters* **2012**, *100*, 20 203512.

[73] G. Lu, K. Yu, Z. Wen, J. Chen, *Nanoscale* **2013**, *5*, 4 1353.

[74] M. F. Craciun, S. Russo, M. Yamamoto, J. B. Oostinga, A. F. Morpurgo, S. Tarucha, *Nature Nanotechnology* **2009**, *4*, 6 383.

[75] O. V. Gamayun, E. V. Gorbar, V. P. Gusynin, *Physical Review B* **2010**, *81*, 7.

[76] X. Yang, G. Liu, M. Rostami, A. A. Balandin, K. Mohanram, *IEEE Electron Device Letters* **2011**, *32*, 10 1328.

[77] H. Li, Q. Zhang, C. Liu, S. Xu, P. Gao, *ACS Nano* **2011**, *5*, 4 3198.

[78] J. F. Tian, L. A. Jauregui, G. Lopez, H. Cao, Y. P. Chen, *Applied Physics Letters* **2010**, *96*, 26 263110.

[79] B. Y. Zhang, T. Liu, B. Meng, X. Li, G. Liang, X. Hu, Q. J. Wang, *Nature Communications* **2013**, *4*, 1.

[80] A. Pospischil, M. Humer, M. M. Furchi, D. Bachmann, R. Guider, T. Fromherz, T. Mueller, *Nature Photonics* **2013**, *7*, 11 892.

[81] M. Liu, X. Yin, E. Ulin-Avila, B. Geng, T. Zentgraf, L. Ju, F. Wang, X. Zhang, *Nature* **2011**, *474*, 7349 64.

[82] S. Cho, M. S. Fuhrer, *Physical Review B* **2008**, *77*, 8.

[83] F. Wang, Y. Zhang, C. Tian, C. Girit, A. Zettl, M. Crommie, Y. R. Shen, *Science* **2008**, *320*, 5873 206.

[84] J. M. Dawlaty, S. Shivaraman, J. Strait, P. George, M. Chandrashekhar, F. Rana, M. G. Spencer, D. Veksler, Y. Chen, *Applied Physics Letters* **2008**, *93*, 13 131905.

[85] K. F. Mak, M. Y. Sfeir, Y. Wu, C. H. Lui, J. A. Misewich, T. F. Heinz, *Physical Review Letters* **2008**, *101*, 19.

[86] G. Xing, H. Guo, X. Zhang, T. C. Sum, C. H. A. Huan, *Opt. Express* **2010**, *18*, 5 4564.

[87] H. Yang, X. Feng, Q. Wang, H. Huang, W. Chen, A. T. S. Wee, W. Ji, *Nano Letters* **2011**, *11*, 7 2622.

[88] G.-K. Lim, Z.-L. Chen, J. Clark, R. G. S. Goh, W.-H. Ng, H.-W. Tan, R. H. Friend, P. K. H. Ho, L.-L. Chua, *Nature Photonics* **2011**, *5*, 9 554.

[89] E. H. Hwang, S. D. Sarma, *Physical Review B* **2007**, *75*, 20.

[90] A. N. Grigorenko, M. Polini, K. S. Novoselov, *Nature Photonics* **2012**, *6*, 11 749.

[91] D. Voiry, A. Mohite, M. Chhowalla, *Chemical Society Reviews* **2015**, *44*, 9 2702.

[92] X. Fan, P. Xu, D. Zhou, Y. Sun, Y. C. Li, M. A. T. Nguyen, M. Terrones, T. E. Mallouk, *Nano Letters* **2015**, *15*, 9 5956.

[93] F. Wypych, R. Schollhorn, *J. Chem. Soc., Chem. Commun.* **1992**, , 19 1386.

[94] R. Ganatra, Q. Zhang, *ACS Nano* **2014**, *8*, 5 4074.

[95] C. Huang, S. Wu, A. M. Sanchez, J. J. P. Peters, R. Beanland, J. S. Ross, P. Rivera, W. Yao, D. H. Cobden, X. Xu, *Nature Materials* **2014**, *13*, 12 1096.

[96] C. Cong, J. Shang, X. Wu, B. Cao, N. Peimyoo, C. Qiu, L. Sun, T. Yu, *Advanced Optical Materials* **2013**, *2*, 2 131.

[97] Y. Zhang, L. Yin, J. Chu, T. A. Shifa, J. Xia, F. Wang, Y. Wen, X. Zhan, Z. Wang, J. He, *Advanced Materials* **2018**, *30*, 40 1803665.

[98] A. Splendiani, L. Sun, Y. Zhang, T. Li, J. Kim, C.-Y. Chim, G. Galli, F. Wang, *Nano Letters* **2010**, *10*, 4 1271.

[99] Y. Yu, J. Yao, X. Niu, B. Xing, Y. Liu, X. Wu, M. Li, X. Yan, J. Sha, Y. Wang, *CrystEngComm* **2020**, *22*, 22 3824.

[100] J. Miao, L. Zhang, C. Wang, *2D Materials* **2019**, *6*, 3 032003.

[101] Y. Yi, Z. Sun, J. Li, P. K. Chu, X.-F. Yu, *Small Methods* **2019**, *3*, 10 1900165.

[102] S. Pandey, A. James, R. Raman, S. Chatterjee, A. Goyal, C. Prakash, T. Goel, *Physica B: Condensed Matter* **2005**, *369*, 1-4 135.

[103] G. Kwei, A. Lawson, S. Billinge, S.-W. Cheong, *The Journal of Physical Chemistry* **1993**, *97*, 10 2368.

[104] M. Klee, R. Mauczok, C. V. Heesch, B. op het Veld, M. D. Wild, H. Boots, B. Kumar, W. Soer, G. Schmitz, M. Mleczko, *Integrated Ferroelectrics* **2012**, *134*, 1 25.

[105] T. Gu, T. Scarbrough, Y. Yang, J. Íñiguez, L. Bellaiche, H. J. Xiang, *Phys. Rev. Lett.* **2018**, *120* 197602.

[106] N. Setter, D. Damjanovic, L. Eng, G. Fox, S. Gevorgian, S. Hong, A. Kingon, H. Kohlstedt, N. Y. Park, G. B. Stephenson, I. Stolitchnov, A. K. Taganstev, D. V. Taylor, T. Yamada, S. Streiffer, *Journal of Applied Physics* **2006**, *100*, 5 051606.

[107] O. I. Prokopalo, A. V. Turik, *Ferroelectrics* **1978**, *22*, 1 749.

[108] J. Jiang, Y. Bitla, C.-W. Huang, T. H. Do, H.-J. Liu, Y.-H. Hsieh, C.-H. Ma, C.-Y. Jang, Y.-H. Lai, P.-W. Chiu, W.-W. Wu, Y.-C. Chen, Y.-C. Zhou, Y.-H. Chu, *Science Advances* **2017**, *3*, 6 e1700121.

[109] D. Páez-Margarit, F. Rubio-Marcos, D. A. Ochoa, A. D. Campo, J. F. Fernández, J. E. Garcá, *ACS Applied Materials & Interfaces* **2018**, *10*, 26 21804.

[110] A. Boes, T. Crasto, H. Steigerwald, S. Wade, J. Frohnhaus, E. Soergel, A. Mitchell, *Applied Physics Letters* **2013**, *103*, 14 142904.

[111] H. Steigerwald, Y. J. Ying, R. W. Eason, K. Buse, S. Mailis, E. Soergel, *Applied Physics Letters* **2011**, *98*, 6 062902.

[112] P. J. Sturman, *Photovoltaic and Photo-refractive Effects in Noncentrosymmetric Materials*, volume 8, CRC Press, **1992**.

[113] T. Li, A. Lipatov, H. Lu, H. Lee, J.-W. Lee, E. Torun, L. Wirtz, C.-B. Eom, J. Íñiguez, A. Sinitskii, A. Gruverman, *Nature Communications* **2018**, *9*, 1.

[114] M.-M. Yang, M. Alexe, *Advanced Materials* **2018**, *30*, 14 1704908.

[115] H. J. Lee, J. Kim, O. Kwon, H. J. Lee, J. H. Kwak, J. M. Kim, S. S. Lee, Y. Kim, D.-Y. Kim, J. Y. Jo, *Applied Physics Letters* **2015**, *107*, 26 262902.

[116] Y. Sun, D. Xie, X. Zhang, J. Xu, X. Li, X. Li, R. Dai, X. Li, P. Li, X. Gao, H. Zhu, *Nanotechnology* **2016**, *28*, 4 045204.

[117] W. Kim, A. Javey, O. Vermesh, Q. Wang, Y. Li, H. Dai, *Nano Letters* **2003**, *3*, 2 193.

[118] J. S. Lee, S. Ryu, K. Yoo, I. S. Choi, W. S. Yun, J. Kim, *The Journal of Physical Chemistry C* **2007**, *111*, 34 12504.

[119] J. Jiang, X. Zou, Y. Lv, Y. Liu, W. Xu, Q. Tao, Y. Chai, L. Liao, *Nature Communications* **2020**, *11*, 1.

[120] L. Liu, L. Wu, A. Wang, H. Liu, R. Ma, K. Wu, J. Chen, Z. Zhou, Y. Tian, H. Yang, C. Shen, L. Bao, Z. Qin, S. T. Pantelides, H.-J. Gao, *Nano Letters* **2020**, *20*, 9 6666.

[121] A. Lipatov, A. Fursina, T. H. Vo, P. Sharma, A. Gruverman, A. Sinitskii, *Advanced Electronic Materials* **2017**, *3*, 7 1700020.

[122] L. Lv, F. Zhuge, F. Xie, X. Xiong, Q. Zhang, N. Zhang, Y. Huang, T. Zhai, *Nature Communications* **2019**, *10*, 1.

[123] C. Baeumer, S. P. Rogers, R. Xu, L. W. Martin, M. Shim, *Nano Letters* **2013**, *13*, 4 1693, pMID: 23506048.

[124] J. Li, Z. Wang, Y. Wen, J. Chu, L. Yin, R. Cheng, L. Lei, P. He, C. Jiang, L. Feng, J. He, *Advanced Functional Materials* **2018**, *28*, 10 1706437.

[125] A. Nguyen, P. Sharma, T. Scott, E. Preciado, V. Klee, D. Sun, I.-H. D. Lu, D. Barroso, S. Kim, V. Y. Shur, A. R. Akhmatkhanov, A. Gruverman, L. Bartels, P. A. Dowben, *Nano Letters* **2015**, *15*, 5 3364.

[126] C. H. Li, K. M. McCreary, B. T. Jonker, *ACS Omega* **2016**, *1*, 6 1075.

[127] C. Baeumer, D. Saldana-Greco, J. M. P. Martirez, A. M. Rappe, M. Shim, L. W. Martin, *Nature Communications* **2015**, *6*, 1.

[128] M. ukaszewicz, P. Guchowski, B. Cichy, W. Strek, *Physics Procedia* **2015**, *76* 155.

[129] Z. Yin, H. Li, H. Li, L. Jiang, Y. Shi, Y. Sun, G. Lu, Q. Zhang, X. Chen, H. Zhang, *ACS Nano* **2011**, *6*, 1 74.

[130] J. Wang, H. Fang, X. Wang, X. Chen, W. Lu, W. Hu, *Small* **2017**, *13*, 35 1700894.

[131] P. L. Richards, *Journal of Applied Physics* **1994**, *76*, 1 1.

[132] N. M. Gabor, J. C. W. Song, Q. Ma, N. L. Nair, T. Taychatanapat, K. Watanabe, T. Taniguchi, L. S. Levitov, P. Jarillo-Herrero, *Science* **2011**, *334*, 6056 648.

[133] N. Huo, G. Konstantatos, *Nature Communications* **2017**, *8*, 1.

[134] J. Chi, N. Guo, Y. Sun, G. Li, L. Xiao, *Nanoscale Research Letters* **2020**, *15*, 1.

[135] F. H. L. Koppens, T. Mueller, P. Avouris, A. C. Ferrari, M. S. Vitiello, M. Polini, *Nature Nanotechnology* **2014**, *9*, 10 780.

[136] R. Zhuo, L. Zeng, H. Yuan, D. Wu, Y. Wang, Z. Shi, T. Xu, Y. Tian, X. Li, Y. H. Tsang, *Nano Research* **2018**, *12*, 1 183.

[137] Y. Liu, J. Wang, H. Huang, Y. Yun, D. Meng, Q. Yang, X. Zhai, Z. Fu, R. J. Knize, Y. Lu, *Advanced Optical Materials* **2017**, *5*, 12 1700158.

[138] E. J. H. Lee, K. Balasubramanian, R. T. Weitz, M. Burghard, K. Kern, *Nature Nanotechnology* **2008**, *3*, 8 486.

[139] K. S. Novoselov, D. Jiang, F. Schedin, T. J. Booth, V. V. Khotkevich, S. V. Morozov, A. K. Geim, *Proceedings of the National Academy of Sciences* **2005**, *102*, 30 10451.

[140] C. Zhou, X. Wang, S. Raju, Z. Lin, D. Villaroman, B. Huang, H. L.-W. Chan, M. Chan, Y. Chai, *Nanoscale* **2015**, *7*, 19 8695.

[141] G. Rao, X. Wang, Y. Wang, P. Wangyang, C. Yan, J. Chu, L. Xue, C. Gong, J. Huang, J. Xiong, Y. Li, *InfoMat* **2019**, *1*, 3 272.

[142] X. Wang, P. Wang, J. Wang, W. Hu, X. Zhou, N. Guo, H. Huang, S. Sun, H. Shen, T. Lin, M. Tang, L. Liao, A. Jiang, J. Sun, X. Meng, X. Chen, W. Lu, J. Chu, *Advanced Materials* **2015**, *27*, 42 6538.

[143] Y. Chen, X. Wang, P. Wang, H. Huang, G. Wu, B. Tian, Z. Hong, Y. Wang, S. Sun, H. Shen, J. Wang, W. Hu, J. Sun, X. Meng, J. Chu, *ACS Appl. Mater. Interfaces* **2016**, *8*, 47 32083.

[144] W. Wu, D. De, S.-C. Chang, Y. Wang, H. Peng, J. Bao, S.-S. Pei, *Applied Physics Letters* **2013**, *102*, 14 142106.

[145] X. Tong, E. Ashalley, F. Lin, H. Li, Z. M. Wang, *Nano-Micro Letters* **2015**, *7,* 3 203.

[146] S. Wu, G. Wu, X. Wang, Y. Chen, T. Lin, H. Shen, W. Hu, X. Meng, J. Wang, J. Chu, *Journal of Semiconductors* **2019**, *40*, 9 092002.

[147] J. Guo, S. Li, Y. Ke, L. Mao, W. Huang, X. Zhang, In H. Wang, editor, *Eleventh International Conference on Information Optics and Photonics (CIOP 2019)*. SPIE, **2019** .

[148] P. Hou, Y. Lv, X. Zhong, J. Wang, *ACS Applied Nano Materials* **2019**, *2*, 7 4443.

[149] B. Liu, B. Tang, F. Lv, Y. Zeng, J. Liao, S. Wang, Q. Chen, *Nanotechnology* **2019**, *31*, 6 065203.

[150] G. L. Frey, S. Elani, M. Homyonfer, Y. Feldman, R. Tenne, *Physical Review B* **1998**, *57*, 11 6666.

[151] G. Cunningham, D. Hanlon, N. McEvoy, G. S. Duesberg, J. N. Coleman, *Nanoscale* **2015**, *7*, 1 198.

[152] K. F. Mak, C. Lee, J. Hone, J. Shan, T. F. Heinz, *Physical Review Letters* **2010**, *105*, 13.

[153] K. K. Kam, B. A. Parkinson, *The Journal of Physical Chemistry* **1982**, *86*, 4 463.

[154] S. Tongay, J. Zhou, C. Ataca, K. Lo, T. S. Matthews, J. Li, J. C. Grossman, J. Wu, *Nano Letters* **2012**, *12*, 11 5576.

[155] Y. Ma, Y. Dai, M. Guo, C. Niu, J. Lu, B. Huang, *Physical Chemistry Chemical Physics* **2011**, *13*, 34 15546.

[156] W. Li, T. Wang, X. Dai, X. Wang, C. Zhai, Y. Ma, S. Chang, *Solid State Communications* **2016**, *225* 32.

[157] H. R. Gutiérrez, N. Perea-López, A. L. Elás, A. Berkdemir, B. Wang, R. Lv, F. López-Urás, V. H. Crespi, H. Terrones, M. Terrones, *Nano Letters* **2012**, *13*, 8 3447.

[158] A. Kuc, N. Zibouche, T. Heine, *Physical Review B* **2011**, *83*, 24.

[159] S. B. Desai, G. Seol, J. S. Kang, H. Fang, C. Battaglia, R. Kapadia, J. W. Ager, J. Guo, A. Javey, *Nano Letters* **2014**, *14*, 8 4592.

[160] L. Brixner, *Journal of Inorganic and Nuclear Chemistry* **1962**, *24*, 3 257.

[161] W. S. Yun, S. W. Han, S. C. Hong, I. G. Kim, J. D. Lee, *Physical Review B* **2012**, *85*, 3.

[162] D. H. Keum, S. Cho, J. H. Kim, D.-H. Choe, H.-J. Sung, M. Kan, H. Kang, J.-Y. Hwang, S. W. Kim, H. Yang, K. J. Chang, Y. H. Lee, *Nature Physics* **2015**, *11*, 6 482.

[163] Y.-F. Lin, Y. Xu, S.-T. Wang, S.-L. Li, M. Yamamoto, A. Aparecido-Ferreira, W. Li, H. Sun, S. Nakaharai, W.-B. Jian, K. Ueno, K. Tsukagoshi, *Advanced Materials* **2014**, *26*, 20 3263.

[164] I. G. Lezama, A. Arora, A. Ubaldini, C. Barreteau, E. Giannini, M. Potemski, A. F. Morpurgo, *Nano Letters* **2015**, *15*, 4 2336.

[165] C. Ruppert, O. B. Aslan, T. F. Heinz, *Nano Letters* **2014**, *14*, 11 6231.

[166] A. Kumar, P. K. Ahluwalia, *The European Physical Journal B* **2012**, *85*, 6.

[167] C.-H. Lee, E. C. Silva, L. Calderin, M. A. T. Nguyen, M. J. Hollander, B. Bersch, T. E. Mallouk, J. A. Robinson, *Scientific Reports* **2015**, *5*, 1.

[168] D. Mao, B. Du, D. Yang, S. Zhang, Y. Wang, W. Zhang, X. She, H. Cheng, H. Zeng, J. Zhao, *Small* **2016**, *12*, 11 1489.

[169] S. Samanta, M. Rath, V. Sankaranarayanan, K. Sethupathi, M. S. R. Rao, *physica status solidi (b)* **2019**, *257*, 1 1900272.

[170] Y. H. Paik, H. S. Kojori, J.-H. Yun, S. J. Kim, *Materials Letters* **2016**, *185* 247.

[171] M. Zhu, Z. Du, H. Li, B. Chen, L. Jing, R. Y. J. Tay, J. Lin, S. H. Tsang, E. H. T. Teo, *Applied Surface Science* **2017**, *425* 1059.

[172] R. S. Ganesh, S. K. Sharma, N. Abinnas, E. Durgadevi, P. Raji, S. Ponnusamy, C. Muthamizhchelvan, Y. Hayakawa, D. Y. Kim, *Materials Chemistry and Physics* **2017**, *192* 274.

[173] D. Sando, C. Carrétéro, M. N. Grisolia, A. Barthélémy, V. Nagarajan, M. Bibes, *Advanced Optical Materials* **2017**, *6*, 2 1700836.

[174] L. Qiao, S. Zhang, H. Y. Xiao, D. J. Singh, K. H. L. Zhang, Z. J. Liu, X. T. Zu, S. Li, *Journal of Materials Chemistry C* **2018**, *6*, 5 1239.

[175] T. Onaya, T. Nabatame, N. Sawamoto, A. Ohi, N. Ikeda, T. Nagata, A. Ogura, *Microelectronic Engineering* **2019**, *215* 111013.